WELDABILITY OF DISTRICT HEATING APPLICATIONS

REPORT 2023-982

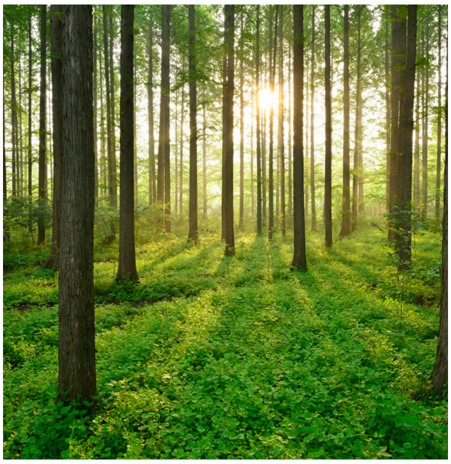

FUTUREHEAT

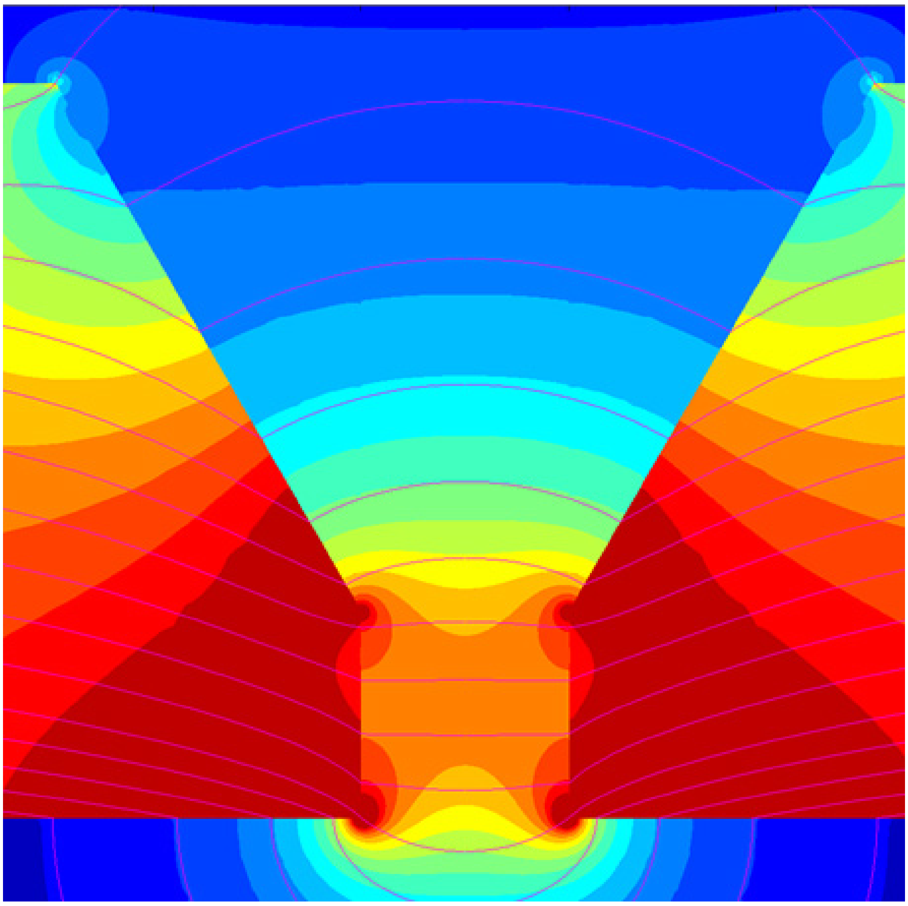

Energiforsk

Weldability of district heating applications

JOAR DRAXLER, LARS-ERIK STRIDH
JOEL ANDERSSON

ISBN 978-91-7673-982-2 | © Energiforsk december 2023
Energiforsk AB | Telefon: 08-677 25 30 | E-post: kontakt@energiforsk.se | www.energiforsk.se

Foreword

Several Swedish district heating companies have reported an increased challenge in implementing approved welding joints for welding district heating pipes in recent years. The issue is being investigated within the project 'Weldability of District Heating Application,' and the causes and proposed solutions are being presented.

The project has been led and carried out by Joel Andersson, Joar Draxler, and Lars-Erik Stridh from Högskolan Väst.

A reference group comprising Magnus Ohlsson from Öresundskraft (coordinator), Martin Lindner from Tekniska Verken in Linköping, Anders Fransson from Göteborg Energi, and Harald Svensson from E.ON has participated and ensured the quality of the project.

This project is part of the Futureheat program, aiming in the long term to contribute to the vision of a sustainable heating system with successful companies leveraging new technical opportunities and optimizing community investments in district heating and cooling. It is within the second phase of the program.

The program is guided by a steering group consisting of Jonas Cognell from Göteborg Energi (Chairman); Anders Moritz from Tekniska Verken in Linköping; Anna Hinderson from Vattenfall AB; Charlotte Tengborg from E.ON Värme Sverige; Fabian Levihn from Stockholm Exergy; Holger Feurstein from Kraftringen; Dan Bruhn from Jönköping Energy; Johan Brossberg from Borlänge Energy; Leif Bodinson from Söderenergi; Lena Olsson Ingvarson from Mölndal Energy; Magnus Ohlsson from Öresund Force; Niklas Lindmark from Gävle Energy; Per Örvind from Eskilstuna Strängnäs Energy & Environment; Petra Nilsson from Växjö Energy; Staffan Stymne from Northern Energy; Stefan Hjärtstam from Borås Energy and Environment; Svante Carlsson from Skellefteå Kraft; Ulf Lindquist from Jämtkraft; and Julia Kuylenstierna (adjunct) from Energiforsk.

Alternates are Ann Britt Larsson from Tekniska Verken in Linköping, Patrik Grönbeck from Borlänge Energy, and Peter Rosenkvist from Gävle Energy

Carolina Holmberg, Program Manager FutureHeat

These are the results and conclusions of a project, which is part of a research programme run by Energiforsk. The author/authors are responsible for the content.

Summary

This report studies residual magnetism in pre-insulated district heating pipes that can lead to difficulties when the pipes are to be welded together at a field, shaft or other workplace. When the residual magnetization is strong enough, it can affect the arc of the weld, which can lead to arc instability and arc deflection. This makes the arc difficult to control for the welder and can thus create welding defects such as bonding errors, porosity and slag inclusions.

The report presents a numerical model developed to study magnetic fields in and around steel pipes. The model has been calibrated against several magnetic hysteresis for P235GH, which is a common steel grade for district heating pipes. The model has been used to investigate the strength required of an external magnetic field to magnetize a district heating pipe to a level that can lead to arc instability and arc deflection. The model has also been used to calculate the amplification that takes place of the magnetic field in the weld groove when two magnetized pipes are brought together. Furthermore, the model has been used to investigate the degree of residual magnetism that can form in a district heating pipe due to the earth's and electric power lines' magnetic fields. The dependence of the magnetic field strength in the weld groove on variations in pipe dimensions and gap geometry has also been simulated.

Furthermore, a measuring method is presented for quickly and robustly measuring the magnetic field at pipe ends and in welding grooves between district heating pipes. The method has been used to measure the residual magnetism in DN600, DN400 and DN300 pipes. Measurements have also been done to investigate whether residual magnetism can form in district heating pipes due to the pipe insulation process and from the joining process by welding. For the DN250 and DN150 pipes examined, both processes had little effect on the residual magnetism.

An experimental set-up developed to investigate threshold values for the level of residual magnetism required to cause arc instability and arc deflection is also presented in the report. With this setup, arc instability and arc deflection were shown to occur in DN150 pipes when the residual magnetization reached to approximately 20 and 40 Gauss, respectively.

The report presents a study that shows that there are steel mills in Europe (manufacturers of, among other things, steel pipes for district heating pipes) that use non-destructive testing methods that can give rise to strong residual magnetism. When such methods are used, the pipes must be demagnetized afterwards. However, it has been shown that the approved levels to which it is demagnetized are too high to completely rule out that arc deflection can occur. To remedy this, a reduction of the maximum permissible level of residual magnetism in the technical regulation D: 211 will be carried out. The hope is that this can lead to steel mills demagnetizing to lower levels than current levels, and that the problems with residual magnetism in district heating pipes can thus be reduced. Modification work with the technical regulation D: 211 will be carried out in a continuation project.

Summary (extended)

In this research project, the residual magnetism in pipes for district heating is studied. This can lead to difficulties when the pipes are welded together. When the residual magnetism is strong enough, it can interact with the electrical arc created by welding, which can result in arc instability and deflection of the arc. For the operator, this makes the welding difficult to control and can therefor create welding defects like lack of fusion, porosity and slag inclusions.

The report presents a numerical model, developed to study magnetic fields in, and around steel pipes. The model has been used to investigate the strength needed from an external magnetic field, in order to magnetise a pipe aimed for district heating, to a level that will result in arc instability and arc deflection. The model has also been used to calculate the reinforcement that occurs in the weld joint, when two magnetised pipes are brought together for welding. Figure 1 shows the field lines when the pipes have been joined to the proper root gap, 2 mm. As can be seen, the magnetic field is strongest at the corners of the root face.

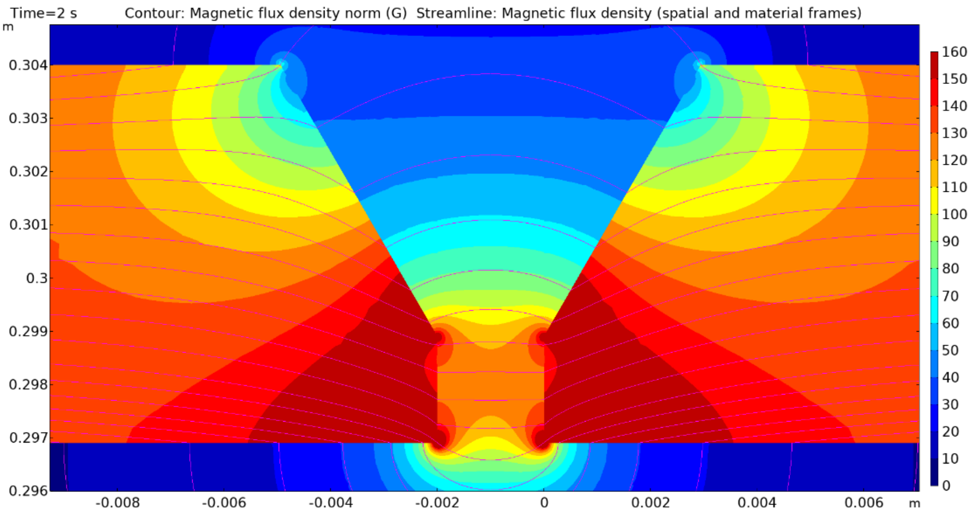

Figure 1. Contour plot and streamlines of the calculated magnetic field at weld groove.

Further on, the model has been used to investigate the degree of residual magnetism that can occur in a pipe for district heating due to the earth's magnetic field and the magnetic field around airborne electrical conduits. The model shows that if the pipe is oriented perpendicularly to the earth's meridian lines, then turned to align with the lines and then back to perpendicular again, the maximum strength in the root opening can reach just below 1 Gauss. Figure 2 below illustrates this result. Results from welding trials show that at the level of approximately 20 Gauss in the root opening, the operator starts to realise the influence of the magnetic field. It is still possible to handle but below this level it is no problem. Thus the magnetization from the earth's magnetic field should not influence the arc.

Energiforsk

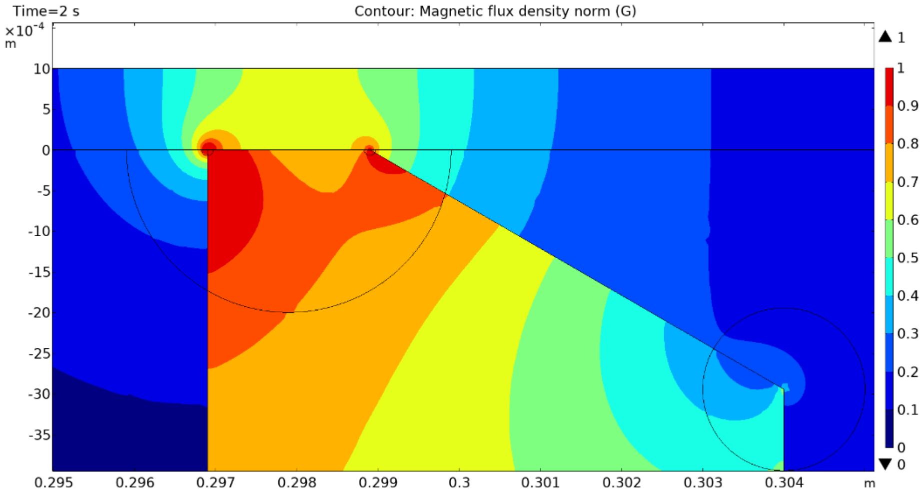

Figure 2. Contour plot of the computed magnetic field at the weld groove of a pipe that has been magnetized by the earth's magnetic field.

In the same way it has been investigated if airborne electrical conduits could result in residual magnetism in the pipes, when transported or parked underneath. The model is not really aimed for this purpose as the magnetic field from a high voltage line is time variating, in addition there is a time variating electrical field around the line, all of which our model does not take into consideration. Nevertheless, we have run simulations with a uniform background field, based on maximum current consumption during the month of February. This results in a maximum magnetic field of 1,5 Gauss in the root opening. This is far below any interference of the arc. This can be seen in Figure 3 below.

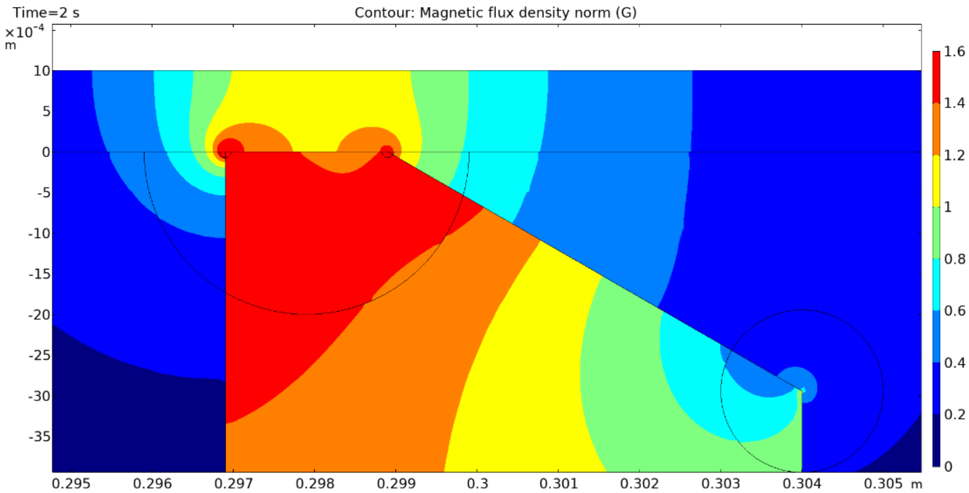

Figure 3. Contour plot of the computed magnetic field at the weld groove of a pipe that has been magnetized by a magnetic field from high power airborne electrical conduits.

The magnetic fields dependence of dimensional variations from the pipe and the joint geometry has also been investigate; the results from this can be found in chapter 3.6.

In order to measure the magnetic field at the pipe ends and in the weld joint, a robust method must be used due to high gradients in the magnetic field. For this purpose, a stable and exact stand was designed and produced to hold the probe for the magnetic field meter (Magmeter MF300H+). The probe holder can be adjusted in height with the accuracy of a hundred of a mm, verified by a Mituoyo micrometre built into the stand. The instrument can be seen in Figure 4 below.

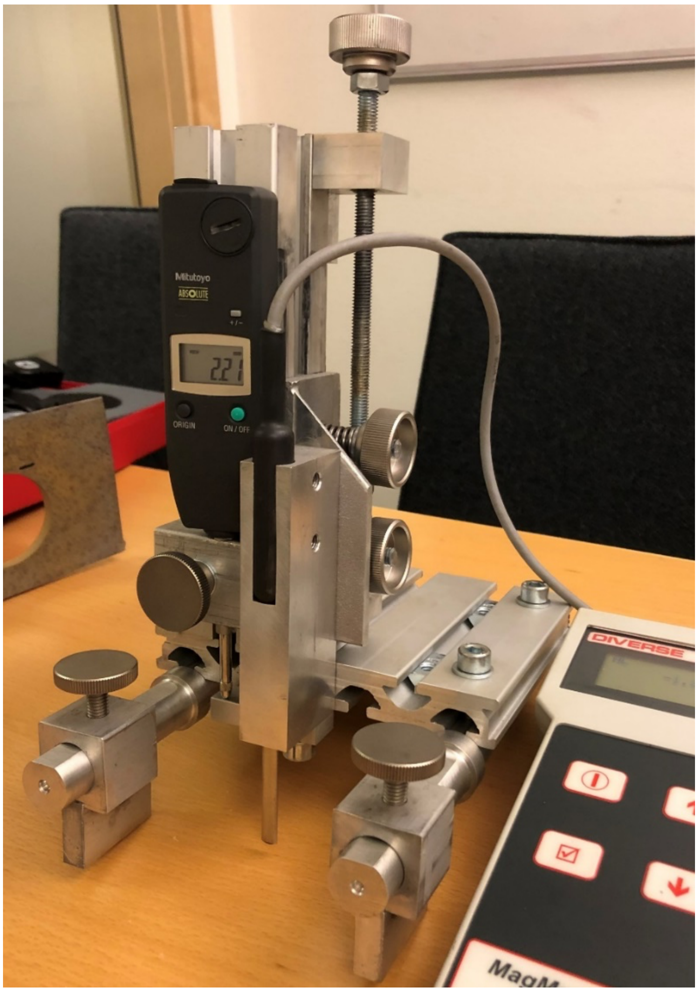

Figure 4. Probe holder.

Practical trails were developed to investigate the threshold values for the residual magnetism, in order to find the values, it takes to cause arc instability and arc deflection. This is presented in chapters 4.2 and 5.3. In Figure 5 below, the weld trial set up is shown. In the trials, we welded on DN150 pipes, residual magnetism of 0, 20, 30 and 40 Gauss were tested, results are also found in the report.

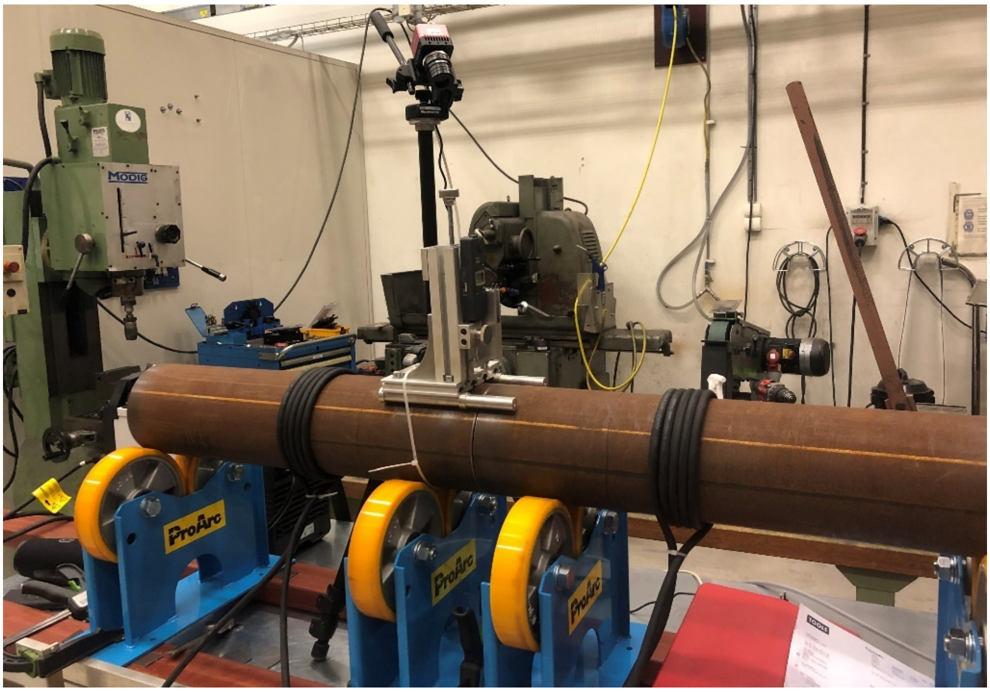

Figure 5. Weld trial set up.

In short, we used two spools around each pipe, these were fed with direct current from a power source (EWM Degauss 600), the current (Amp) was adjusted till the desired level of magnetism in the joint was reached. The magnetic field in the joint, created with this method only has very small variations in the circular direction; maximum variation of B_z in circular direction was only one or two Gauss when the magnetisation was between 5 – 100 Gauss. The created magnetic field had no time dependency: as soon as the magnetic field had been adjusted to a given level, that level was kept constant for more than 10 min (which were the control time) without having to adjust the current in the spools.

The process of insulating the pipes was also investigated by a visit to a district pipe insulating company. In this specific case five different DN250 pipes were tested by using the probe stand described earlier. The magnetic field were checked before the insulation process and after. Each pipe was carefully marked so we could assure that we made the measurements on the exact same pipes after the insulation process. The difference in the magnetic field before and after insulation for all five pipes were all within +/- 3 Gauss for both ends of the pipes. The conclusion of this is that the insulation process is not inducing any large magnetic field to the pipes.

Magnetisation as a result of welding has also been under discussion as the cause of creating residual magnetism. To investigate this, two 700 mm long DN 150 pipes were welded together. First the root run, then after cooling to room temperature, the magnetic field was measured at four location in each end of the pipes. Then the final run was made and again after cooling to room temperature, measurement of the magnetic field as done in exact the same spots. The result was that it varied

Energiforsk

only between 1- 2 Gauss, conclusion is that the welding process is not causing any magnetic fields.

This research project has clearly shown that residual magnetism is an issue that needs to be considered in a more serious way than it has been before. Looking at standards, very little can be found regarding recommendations and regulations of the residual magnetism. From the viewpoint of the pipe producers there is no standard to follow regarding the levels of residual magnetism. This is something that is the task of standardisation organs to take a deeper look into and possibly introduce in the standards for pipe production. There are equipment's available on the market to be used in pipe production with the aim to reduce magnetism to a specific level.

Future work within this research project is most certainly to do more practical experiments for pipes of different diameters and wall thicknesses to find their threshold values for residual magnetism that will cause welding problems.

Sammanfattning

I denna rapport studeras restmagnetism i förisolerade fjärrvärmerör som kan leda till svårigheter då rören skall svetsas samman i fält, schakt eller på annan arbetsplats. Då restmagnetiseringen är stark nog kan den påverka svetsens ljusbåge, vilket kan leda till ljusbågsinstabilitet och ljusbågsavlänkning. Detta gör ljusbågen svårkontrollerbar för svetsaren och kan därmed skapa svetsdefekter som bindfel, porositet och slagginneslutningar.

I rapporten presenteras en numerisk beräkningsmodell som utvecklats för att studera magnetfält i och omkring stålrör. Modellen har kalibrerats mot flera magnetiska hysteres för P235GH, vilket är en vanligt förkommande stålsort till fjärrvärmerör. Modellen har använts för att undersöka styrkan som krävs hos ett externt magnetfält för att magnetisera ett fjärrvärmerör till en nivå som kan leda till ljusbågsinstabilitet och ljusbågsavlänkning. Modellen har också använts för att beräkna förstärkningen som sker av magnetfältet i svetsspalten då två magnetiserade rör förs samman. Vidare har modellen använts för att undersöka graden av restmagnetism som kan uppstå i ett fjärrvärmerör på grund av jordens och elkraftledningars magnetfält. Beroendet av magnetfältets styrka i svetsspalten på variationer i rördimensioner och spaltgeometri har också simulerats.

Vidare presenteras en mätmetod för att snabbt och robust mäta magnetfältet vid rörändar och i svetsspalter mellan fjärrvärmerör. Metoden har använts för att mäta restmagnetismen i DN600, DN400 och DN300 rör. Mätningar har också utförts för att undersöka om restmagnetism kan uppstå på grund av rörisoleringsprocessen och sammansvetsningen av fjärrvärmerör. För de DN250 och DN150 rör som undersöktes hade båda dessa processer liten inverkan på restmagnetismen.

En försöksuppställning som utvecklats för att undersöka tröskelvärden för nivån av restmagnetism som krävs för att orsaka ljusbågsinstabillitet och ljusbågsavlänkning presenteras också i rapporten. Med denna uppställning visades ljusbågsinstabilitet och ljusbågsavlänkning uppstå i DN150 rör när restmagnetiseringen uppgick till ungefär 20 respektive 40 Gauss.

I rapporten presenteras en undersökning som visar att det finns stålverk i Europa (tillverkare av bland annat stålrör till fjärrvärmerör) som använder oförstörande provningsmetoder som kan ge upphov till stark restmagnetism. När sådana metoder används måste rören avmagnetiseras efteråt. Dock har det visat sig att de godkända nivåerna som det avmagnetiseras till är för höga för att helt kunna utesluta att ljusbågsavlänkning kan uppstå. För att åtgärda detta kommer en sänkning av den maximalt tillåtna nivån på restmagnetismen i den tekniska bestämmelsen D:211 att utföras. Förhoppningen är att detta kan leda till att stålverk avmagnetiserar till lägre nivåer än dagens nivåer, och att därmed problemen med restmagnetism i fjärrvärmerör kan minskas. Förändringsarbete med den tekniska bestämmelsen D:211 kommer att utföras i ett fortsättningsprojekt.

List of content

1 Introduction

The method of joining pipe lengths to pipelines by fusion welding has existed for a very long time. Initially, gas welding, using oxygen and acetylene to melt the joint surfaces and a filler material, was the predominant method. However, when the coated electrode was developed for electric arc welding (1904), this method was switched to. At first, alternating current was used when welding with coated electrodes, and there were no issues with magnetic disturbances in the arc. During the latter part of the 20th century, people switched more and more to welding with direct current, and today, mostly all welding is done with direct current.

With this transition to direct current, a magnetic field is obtained around the arc which, unlike the magnetic field around an alternating current arc, does not change direction 50 times/sec (the frequency is 50 Hz), but always has the same direction. This means that if there is residual magnetism in the base material to be butt-welded, it will give a concentration of the field lines over the straight edge of the weld joint, which can become so strong that the arc is deflected and becomes unstable.

1.1 STRUCTURE OF THE REPORT

Initially, the problems and background with arc instability and deflection are described, along with their consequences for quality and the operator. Possible causes of the residual magnetism in pipes are discussed and the two main concepts for manufacturing pipes are described, possible reasons for residual magnetism being induced in the pipes by the two methods are highlighted. The welding methods are important, and being described and discussed.

The numerical simulation developed for the project is reported in detail including all conditions, formulas and models. The calibration based on the experimental data has been carefully executed. This simulation model is utilized to investigate external factors that have been discussed as possible causes of residual magnetism, and the findings are presented. Additionally, the physical differences in the dimensions of the pipes and joint designs are evaluated using the simulation tool.

Practical experiments and investigations have been conducted, and the results are presented in tables, accompanied by images and explanations. All the processes that the pipes undergo after manufacturing have been examined. Although visits to pipe manufacturers were not conducted, a questionnaire has been sent, and the responses are reported in the document.

Finally, various proposed actions are discussed aiming at minimizing the problems of arc deflection and welding instability. Besides, our conclusions are reported with suggestions for further work, which includes investigation with the pipe manufacturers and larger pipe diameter and thickness.

1.2 BACKGROUND

The deflection and instability described in the introduction can be over the limit the welder being able to compensate and results in welding defects. The defects we may encounter are lack of fusion, slag inclusions, and undercut. A lack of fusion occurs when the arc deflection to the extent that it does not melt the joint surface, and the melted filler metal from the electrode only lays on the surface without metallurgical bonding with the base material. With such defects, the joint has no strength.

Slag inclusions can occur when the easily flowing slag, formed by the electrode's coating, flows into the molten weld pool due to an unstable arc and gets trapped between the molten metal and the base material. The same, there is no bonding between the weld material and the base material. Undercut refers to a groove, just as the name suggests, in the transition between the base material and the weld metal. It could be a few millimeters wide and deep. It needs to be ground off and repaired; otherwise, a defect will occur when the next weld bead passes over it.

But none of these problems would have arisen if the pipes did not have a residual magnetism. This phenomenon or problem is something that has increased in the last 5 – 10 years and the question is why. It has nothing to do with the electrode (filler material) itself; it has not changed in any way. It probably does not have anything to do with the power sources either, even though they have undergone a dramatic change in the past 20 years, transitioning from welding transformers to rectifiers with diode bridges, then to inverters with transistor rectifiers, and today fully electronic power sources.

What may have changed is the methods used for testing the pipes during manufacturing. Nowadays, magnetic particle testing or eddy current testing is commonly employed. Both of these methods require the demagnetization of the pipes after testing. The problem lies in the fact that standards and norms do not specify the degree of demagnetization must reach.

Often, the residual magnetism remains at around 20-30 Gauss, which has been found to be too high in our experiments.

1.3 WELDING OF DISTRICT HEATING APPLICATION

As mentioned earlier, gas welding (oxygen and acetylene) was previously used for field welding of pipe joining during pipeline installation. However, except for smaller pipe dimensions, this method has been replaced by shielded metal arc welding (SMAW) using coated electrodes. With modern lightweight power sources, SMAW has become a highly flexible method with minimal 'setup time'. In some pipeline welding applications, mechanized welding is used with either TIG welding which is set up in orbital welding equipment, or similar systems for gas metal arc welding (MIG/MAG). It makes the welder and operator easier by using the equipment carrying, managing, and monitoring the process. However, working outdoors presents such challenges as the needs of protection from weather conditions and wind, and there is increased down-time in 'pipe trench'.

Therefore, for the foreseeable future, field installation of district heating pipes will likely continue using coated electrodes for welding.

1.4 ARC INSTABILITY AND ARC DEFLECTION

In arc welding, a very hot plasma is formed between the cathode and the anode. The plasma consists of an ionized gas which in turn consists of positively charged ions and negatively charged electrons [1]. These charged particles move at very high speeds in the plasma. As the charged particles are in motion, they form an electric current in the plasma that induces a magnetic field.

As the workpiece is magnetic, i.e. has a residual magnetism, this magnetic field can interact with the magnetic field in the plasma. If the residual magnetism is strong enough, its interaction with the plasma can be so powerful that it makes the plasma unstable, and thus arc instability problems can arise. The residual magnetism also gives rise to a deflection (bending) of the plasma by $\mathbf{E}\times\mathbf{B}$-drift, where the plasma is linked by perpendicular to the electric field, $\mathbf{E}$, and perpendicular to the magnetic field, $\mathbf{B}$ [2]. The residual magnetism also gives rise to a diamagnetic-drift which by the plasma perpendicular to the $\mathbf{B}$ -field and $\boldsymbol{\nabla} p$ - the gradient, where p is a plasma pressure [2]. If the residual magnetism is strong enough, this can lead to a strong deflection of the plasma, leading to problems with arc deflection.

Arc instability and arc deflection make it difficult for the welder to control the arc. This can lead to insufficient fusion of the sidewalls, which in turn can lead to bond failure. The uncontrollable arc can also lead to slag inclusions, uneven transition and heavy spatter. When the arc is heavily deflected, it can be challenging to ensure proper shielding gas coverage of the molten pool, which can result in issues such as porosity.

The sensitivity of the arc to being affected by an external magnetic field depends on the welding current and welding voltage (among other things). A higher welding current and voltage gives a more stable arc. This means that different welding methods are differently sensitive to arc instability and arc deflection. For example, TIG welding tends to be more sensitive to arc deflection than MIG and MMA welding due to the lower arc voltage. Guidelines for the level of residual magnetism required to cause arc instability and arc deflection, for various welding methods, are reported by, among others, the companies Diverse Technologies & Systems Ltd [3], see Table 1 below, and EWM AG [4], see Table 2 below. Note that these are only general guidelines, the actual values depend on the welding current, welding voltage, shielding gas/electrode type, welding method (DC or AC), material composition, etc.

Table 1. Threshold values for arc instability and arc deflection for different welding methods, from Diverse Technologies & Systems Ltd [3].

Welding process	0 – 10 gauss	10 – 20 gauss	20 – 40 gauss	over 40 gauss
TIG	normal welding	arc instability	arc blow	severe arc blow
Manual metal arc	normal welding	normal welding	arc instability	arc blow
Submerged arc	normal welding	normal welding	normal welding	arc instability

Table 2. Threshold values for arc instability and arc deflection for different welding methods, from EWM AG [4].

Recommended values for TIG welding		Recommended values for MIG/MAG welding	
Field strength	**Result**	**Field strength**	**Result**
< 0,5 mT	★★★★	< 3 mT	★★★★
0,5-1 mT	★★★☆	3-4 mT	★★★☆
1-2 mT	★★☆☆	4-6 mT	★★☆☆
2-5 mT	★☆☆☆	6-8 mT	★☆☆☆
> 5 mT	☆☆☆☆	> 8 mT	☆☆☆☆

1.5 RESIDUAL MAGNETISM

District heating pipes are usually made of low-alloy steels that are soft ferromagnetic. Ferromagnetic materials can have a permanent magnetization without the presence of an external magnetic field [5]. For a soft ferromagnetic material, it can be demagnetized with a relatively weak external magnetic field, compared to a hard ferromagnetic material, such as permanent magnets, which requires a strong external magnetic field to be demagnetized.

Ferromagnetic materials consist of magnetic domains which are small areas in microscopical scale. In the magnetic domain, all magnetic moments are parallel. The magnetic moments arise from the spins of electrons, and in a magnetic domain all the spins point in the same direction. A ferromagnetic material is in its lowest energy state when its magnetic domains are randomly oriented. The random orientation results in the macroscopic magnetization of the material turning to zero. By applying an external magnetic field, for example, the magnetic domains can align themselves according to the field's direction. This occurs through domain rotation and by favorably oriented domains growing at the expense of unfavorably oriented domains, as shown in Figure 1 below.

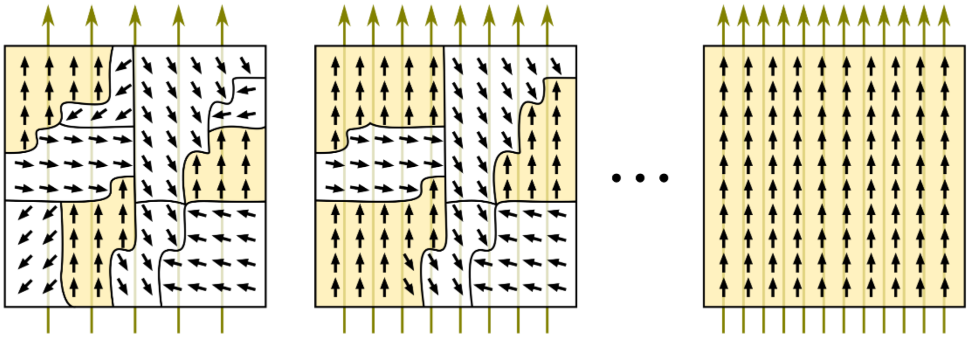

Figure 1. Rotation of orientation and increased size of magnetic domains in response to an externally applied magnetic field. From [6].

When the external magnetic field is removed, the material remains magnetized because the net magnetization is no longer zero. This state does not correspond to the lowest energy state and is therefore quasi-static, but it could take a very long time for the material to return to its lowest energy state and for the magnetization to disappear. Ferromagnetic materials can also be magnetized through plastic deformations, for example.

1.6 STEEL PIPE MANUFACTURING

1.6.1 Manufacturing process

The manufacturing concepts used for pipes are either longitudinally welded pipes or spirally welded pipes. If we start with the longitudinally welded pipes, they are manufactured in specific lengths, normally 6, 8, 10, 12 even up to 16 m. It is most common that pipes with a thickness of less than 12 mm are made with this method. The principle involves the use of a large and long press with an upper roll and two lower rolls where the distance from each other can be continuously adjusted. The sheet metal, already prepared for joints and adjusted to the correct length, is inserted between the rollers and a pressure is applied to the upper roller. The plate is rolled back and forth between the rolls while increasing pressure on the upper roll. Once the desired diameter is achieved, the "pipe" is taken out from the rolls and processed in various ways to approach the specified dimensional tolerances as closely as possible. Finally, the longitudinal joint is welded, both from the outside and the inside, depending on the plate thickness and diameter.

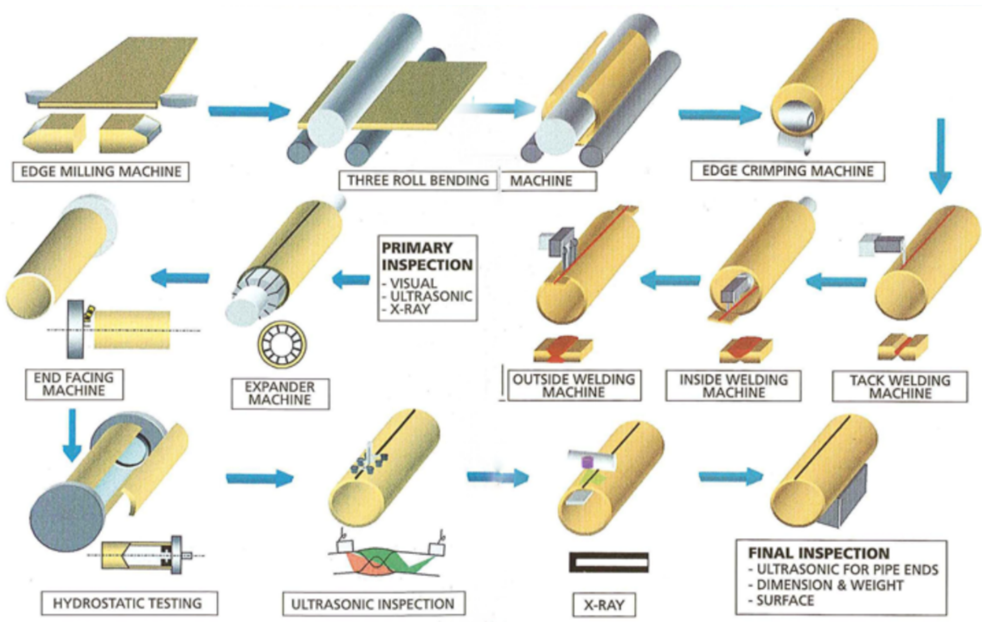

Figure 2. Manufacturing process for longitudinally welded steel pipes. From [7].

Spiral welded pipes are made in diameters from approx. 100 mm up to approx. 2,500 mm. The thickness of the pipes is normally limited to 25 mm. This is a process which is often continuous, i.e. the pipe is made infinitely long and flying cutters make sure to cut the pipe into desired lengths. The process begins with a coiled sheet which, at a specific angle depending on the desired diameter, is fed into a sheet forming machine where the sheet is shaped by rollers into a circle. Both inside and outside the pipe, welding equipment is situated, continuously welding the inside first and then the outside, completing half a rotation. When the sheet in the reel running out, a new reel is quickly placed in position and welded on-the-fly in the straight section before the rolling. This allows the process to run continuously.

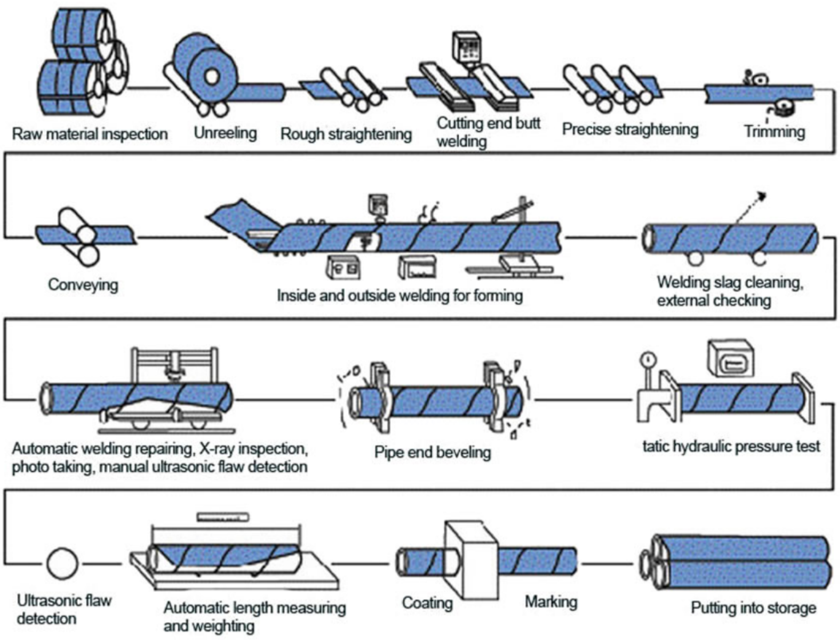

Figure 3. Manufacturing process for spiral welded steel pipes. From [8].

1.6.2 Welding method

In the manufacturing of pipes, mainly two welding methods are used. For tack welding of joints and welding of thin-walled pipes, gas metal arc welding with solid wire or metal powder-filled wire is employed. The process can utilize single-wire, twin-wire, or tandem systems. For material thicknesses of approximately 10 mm and above, powder arc welding is primarily used. This method is highly productive and depending on the thickness and diameter of the material, up to 6 wires can be used in the same molten pool. With this configuration, deposition rates of up to 105 kg/h can be achieved. In more modern pipe manufacturing facilities, laser welding is also used, as well as a combination of laser and powder arc welding, and in some cases, laser with gas metal arc welding.

1.6.3 Residual Magnetism from Pipe Manufacturing

Residual magnetism can occur in steel pipes through various means, especially during the pipe manufacturing process. Here is a list of some possible causes of residual magnetism:

- Magnetic clamping and lifting tools.
- Plasma cutting (used by some pipe manufacturers to cut pipes to the correct length).
- Magnetized non-destructive testing. Testing methods like magnetic particle inspection and saturation eddy current testing can result in strong residual magnetism.
- Descaling and shaping of the steel plate into a pipe. This is associated with plastic deformations, which can lead to residual magnetism.
- Joint preparation, grinding, and other machining methods.
- Longitudinal or spiral welding of the steel pipe.

- Direct contact with heavily magnetized objects such as bending rolls.

2 Numerical simulation

In this chapter, a numerical model is described that has been developed to study the magnetic field in the weld gap between two district heating pipes. The model is based on the Jiles-Atherton constitutive relationships, which have been calibrated against several magnetic hysteresis curves for the steel grade P235GH. The model is magnetostatic, as no free electric currents or time-varying magnetic fields are assumed to be present. The model is also axisymmetric, which significantly reduces computational complexity compared to a full 3D model. This enables the use of a fine mesh to resolve the magnetic field, especially in areas like corners where large gradients occur. The model and its setup in the computational software COMSOL [9], [10].

2.1 MAGNETOSTATIC

Consider a magnetized steel pipe with no free electric currents or rapidly time-varying magnetic fields. Under these assumptions, Maxwell's equations are reduced to [11]

$$\begin{cases} \nabla \cdot \mathbf{B} = 0 \\ \nabla \times \mathbf{H} = \mathbf{0} \end{cases} \tag{2.1}$$

where $\mathbf{B}$ is the magnetic flux density and $\mathbf{H}$ is the magnetic field strength. By definition, the $\mathbf{B}$ and $\mathbf{H}$ has the relationship according to [11]

$$\mathbf{H} = \frac{\mathbf{B}}{\mu_0} - \mathbf{M} \tag{2.2}$$

Where $\mathbf{M}$ is the magnetization vector field, and μ_0 is the permeability of vacuum. Furthermore, according to the Helmholtz theorem, any smooth vector field can be written as the sum of an irrotational vector field and a divergence-free vector field. Since an irrotational vector field has a scalar potential and a divergence-free vector field has a vector potential, the Helmholtz theorem states that $\mathbf{H}$ can be written as [11]

$$\mathbf{H} = -\nabla V + \nabla \times \mathbf{A} \tag{2.3}$$

where V is a scaler potential and $\mathbf{A}$ is a vector potential. Since $\nabla \times \mathbf{H} = \mathbf{0}$ according to (2.1)b, i.e. irrotational, it must be $\nabla \times \mathbf{A} = \mathbf{0}$ in equation (2.3), which then reduces to

$$\mathbf{H} = -\nabla V \tag{2.4}$$

Let us now consider a given background field $\mathbf{H}_b$ which is used to magnetize the steel pipes. $\mathbf{H}$ can then be written as a sum of $\mathbf{H}_b$ and a reduced field $\mathbf{H}_{red}$

$$\mathbf{H} = \mathbf{H}_{red} + \mathbf{H}_b \tag{2.5}$$

where $\mathbf{H}_{red}$ is unknown. From equation (2.4) it can be deduced that $\mathbf{H}$ can be determined from a reduced scalar potential as follows

$$\mathbf{H} = -\nabla V_{red} + \mathbf{H}_b \tag{2.6}$$

By substituting equation (2.6) into equation (2.2), and then substituting equation (2.2) in equation (2.1)a, obtains

$$\mu_0 \nabla \cdot (-\nabla V_{red} + \mathbf{H}_b) + \mu_0 \nabla \cdot \mathbf{M} = 0 \quad (2.7)$$

In Chapter **Fel! Hittar inte referenskälla.** a constitutive relationship is presented where $\mathbf{M}$ can be expressed as a function of $\mathbf{H}$. As $\mathbf{H}$, in turn, can be written as a function of V_{red} according to equation (2.6), this constitutive relationship implies that V_{red} is the only dependent variable that is unknown in equation (2.7). By solving equation (2.7) for V_{red} , then $\mathbf{H}$, $\mathbf{M}$, and $\mathbf{B}$ can be determined.

2.2 BOUNDARY CONDITIONS

At the boundary layer between the steel pipe and its surrounding air, the tangential component of $\mathbf{H}$ is continuous [11], i.e.

$$\mathbf{n}_{12} \times (\mathbf{H}_2 - \mathbf{H}_1) = \mathbf{0} \quad (2.8)$$

where $\mathbf{H}_1$ and

$\mathbf{H}_2$ are the magnetic field strength at the interface of the steel pipe and in the air, respectively. $\mathbf{n}_{12}$ is a unit normal vector to the interface directed towards the air.

The size of the air domain required to determine the magnetic field in the steel pipe is assumed to be so large that the normal component of the reduced magnetic flux density at its outer boundary is zero [11], i.e.

$$\mathbf{n} \cdot (\mathbf{B} - \mathbf{B}_b) = 0 \quad (2.9)$$

where $\mathbf{n}$ is a unit normal vector to the outer edge of the air domain. Since $\mathbf{M} = \mathbf{0}$ in air, equation (2.9) can express $\mathbf{H}$, with help of equation (2.2) and (2.5), as

$$\mathbf{n} \cdot (\mathbf{H} - \mathbf{H}_b) = 0 \quad (2.10)$$

To make the model more computationally efficient, only one of the two pipes is modelled. This is achieved by letting the air domain terminate at the geometric symmetry plane between the two pipes. Along its boundary along this plane, we gets

$$V_{red} = 0 \quad (2.11)$$

This causes the magnetic field to be antisymmetric around the geometric symmetry plane between the two pipes [11]. In this manner, when the magnetic field is antisymmetric, it is sufficient to model only one pipe if the boundary condition in equation (2.11) is used.

By utilizing boundary conditions (2.8), (2.10) and (2.11) equation (2.7) can be solved for V_{red} .

2.3 BACKGROUND FIELD

The pipes are magnetized in the computational model with an axial background field given by

$$\mathbf{H}_b = H_{bp} \mathrm{int1}(t) \hat{\mathbf{e}}_z \quad (2.12)$$

where H_{bp} is the maximum magnitude of the background field. $\text{int1}(t)$ is a function of time, t, with the form of a piecewise cubic polynomial. At $t = 0$, having $\text{int1} = 0$, for $t = 0.5$ s having $\text{int1} = 1$ which is largest, and at $t > 1$ s having $\text{int1} \equiv 0$; see Figure 4a below. The axial background field in the full computational domain is shown in Figure 4b. The vertical axis in the figure is the z-axis.

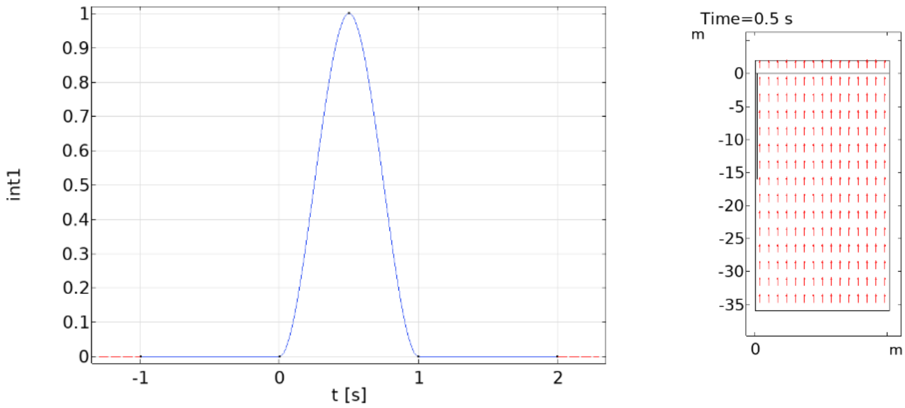

Figure 4. (a) $\mathbf{int1}(\boldsymbol{t})$, (b) the background field in the computational domain. The vertical axis in the figure coincides with the axis of rotation of the axisymmetric model.

2.4 CONSITUTIVE RELATIONSHIP

To solve equation (2.7) , $\mathbf{M}$ must be described as a function of $\mathbf{H}$. This is trivial for air since $\mathbf{M} = \mathbf{0}$ in air. For the steel pipe, it is much more difficult. Several constitutive relationships have been developed for this purpose. In this work, we have chosen to use the Jiles-Atherton (JA) constitutive model [12], which is one of the most popular magnetic hysteresis models. This model is physically based and can be used to calculate both minor and major hysteresis loops. The JA model is implemented in COMSOL according to [9]

$$\begin{cases} \mathbf{H}_e = \mathbf{H} + \alpha \mathbf{M} \\ \chi = \dfrac{1}{k_p}(\mathbf{M}_{an} - \mathbf{M}) \\ \mathbf{M}_{an} = M_s \text{Lan}\left(\dfrac{\|\mathbf{H}_e\|}{a}\right)\dfrac{\mathbf{H}_e}{\|\mathbf{H}_e\|} \\ \dfrac{d\mathbf{M}}{dt} = c_r \dfrac{d\mathbf{M}_{an}}{dt} + \max\left(\chi \dfrac{d\mathbf{H}_e}{dt}, 0\right)\dfrac{\chi}{|\chi|} \end{cases} \tag{2.13}$$

where

$$\text{Lan}(x) = \coth(x) - \frac{1}{x} \tag{2.14}$$

The Langevin function is characterized by the physical parameters M_s, a, k_p, c_r and α which are related to the magnetic properties of the material as follows. M_s represents the saturation magnetization of the material, a quantifies the domain wall density, k_p quantifies the average energy required to overcome pinning sites of magnetic domains in the material, c_r indicates magnetization reversibility, and α quantifies interdomain coupling in the material [12].

2.4.1 Calibration of numerical model

The parameters M_s, a, k_p, c_r and α in the JA-modellen must be determined through calibration against experimental data. The experimental data was obtained from a toroid with a rectangular cross-section that was water-cut from a DN700 district heating pipe with a wall thickness of 8 mm, as shown in Figure 5 below. The toroid's outer and inner diameters are 55 mm and 45 mm, respectively.

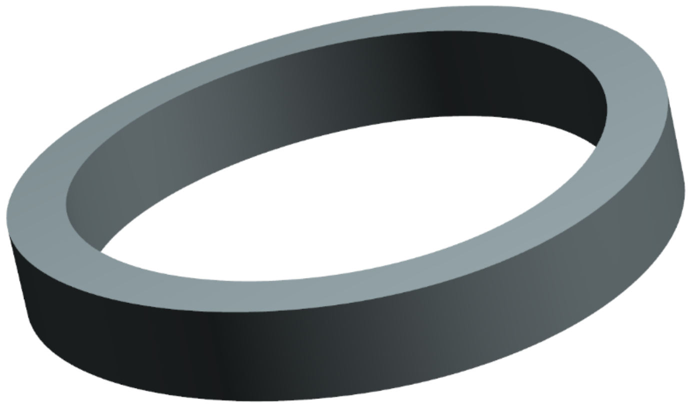

Figure 5. Toroid cut from a DN700 pipe.

The material is P235GH, which is a low-alloy steel with a chemical composition as indicated in Table 3 below. P235GH is a material normally used for district heating pipes.

Table 3. Chemical composition of P235GH [13].

	C	Mn	Si	P	S	Cr	Ni	Mo	Cu
Wt%	≤0.16	0.35	0.6–1.2	≤0.025	≤0.01	≤0.3	≤0.3	≤0.08	≤0.3

The Department of Industrial Production at Lunds University of Technology conducted quasi-static magnetic hysteresis measurements on the toroid. This was achieved by winding the toroid with a primary coil of 60 turns and a secondary coil of 60 turns. The primary coil was used to magnetize the toroid, while the secondary coil was used to determine the magnetic flux density. The current in the primary coil was alternating at a frequency of 0.5 Hz. Figure 6 below displays three measured BH-hysteresis loops for the toroid. The first two loops are minor hysteresis loops obtained from the initially demagnetized toroid. The primary coil was then fed with an alternating current that caused the **H**-field, which can be calculated from the current and the number of turns in the primary coil using Ampere's law, to vary between the extreme values of $\pm Hp$, where Hp = 385 A/m for the hysteresis in Figure 6a and Hp = 766 A/m for the hysteresis in Figure 6b. Both of these are stabilized hysteresis loops, which occur after the current changes direction several times. Figure 6c shows a saturated hysteresis with Hp = 11475 A/m. Hp = 385 A/m is the smallest hysteresis that the employed laboratory was able to generate.

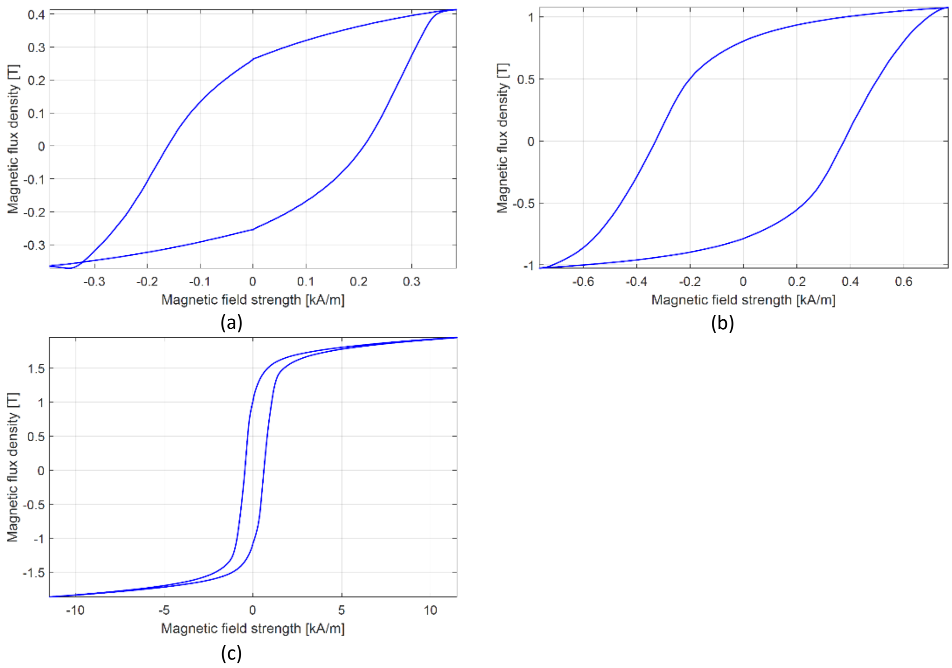

Figure 6. Experimental hysteresis measurements for: (a) Hp= 385A/m, (b) Hp=766 A/m, and (c) Hp= 11475 A/m.

The parameters for the JA model were determined by fitting it to the experimental curves in Figure 6. This is achieved by assuming that the increments on the primary and secondary windings of the toroid are so small that the **H** and **M**-fields are entirely confined within the toroid. Consider now a polar coordinate system with the origin at the midpoint of the toroid. Since **H** and **M** are tangential to the equator of the toroid (according to the previous assumption), only $\hat{\mathbf{e}}_\theta$ components of **H** and **M** differ from zero when expressed in the aforementioned polar coordinate system. Expressed in this system, the only nonzero component of the JA model in equation (2.13) for the toroid can be written as:

$$\begin{cases} H_e = H_d\tilde{H} + \alpha_d\tilde{\alpha}M_d\tilde{M} \\ \chi = \dfrac{1}{k_{pd}\tilde{k}_p}\left(M_{an} - M_d\tilde{M}\right) \\ M_{an} = M_{sd}\tilde{M}_s\left[\coth\left(\dfrac{H_e}{a_d\tilde{a}}\right) - \dfrac{a_d\tilde{a}}{H_e}\right] \\ \dfrac{d\tilde{M}}{d\tilde{t}} = \dfrac{1}{M_d}\left[c_{rd}\tilde{c}_r\dfrac{dM_{an}}{d\tilde{t}} + \max\left(\chi\dfrac{dH_e}{d\tilde{t}}, 0\right)\dfrac{\chi}{|\chi|}\right] \end{cases} \tag{2.15}$$

where

$$\frac{dH_e}{d\tilde{t}} = H_d\frac{d\tilde{H}}{d\tilde{t}} + \alpha_d\tilde{\alpha}M_d\frac{d\tilde{M}}{d\tilde{t}} \tag{2.16}$$

and

$$\frac{dM_{an}}{d\tilde{t}} = \frac{M_{sd}\tilde{M}_s}{a_d\tilde{a}}\frac{dH_e}{d\tilde{t}}\left[1 - \coth^2\left(\frac{H_e}{a_d\tilde{a}}\right) + \frac{(a_d\tilde{a})^2}{H_e^2}\right] \tag{2.17}$$

In equation (2.15) - (2.17), the following dimensionless variables have been used:

$$\widetilde{H} = \frac{H}{H_d}, \qquad \widetilde{M} = \frac{M}{M_d}, \qquad \tilde{t} = \frac{t}{2\pi n} \tag{2.18}$$

This has been done to increase the robustness of numerical integration of these equations. In order to increase robustness in the optimization of the JA parameters, the following dimensionless parameters have also been used in equations(2.15) - (2.17):

$$\widetilde{M}_s = \frac{M_s}{M_{sd}}, \qquad \tilde{a} = \frac{a}{a_d}, \qquad \tilde{k}_p = \frac{k_p}{k_{pd}}, \qquad \tilde{c}_r = \frac{c_r}{c_{rd}}, \qquad \tilde{\alpha} = \frac{\alpha}{\alpha_d} \tag{2.19}$$

The values of the scale parameters used in (2.18) and (2.19) are given in Table 4 below. Its values are chosen so that the variables in (2.18) and (2.19) have a magnitude close to 1.

Table 4. Values of scale parameters.

$\boldsymbol{H_d}$ [A/m]	$\boldsymbol{M_d}$ [A/m]	$\boldsymbol{n}$ [-]	$\boldsymbol{M_{sd}}$ [A/m]	$\boldsymbol{a_d}$ [A/m]	$\boldsymbol{k_{pd}}$ [A/m]	$\boldsymbol{c_{rd}}$ [-]	$\boldsymbol{\alpha_d}$ [-]
1000	10^6	1 – 10	10^6	100	100	0.1	10^{-4}

Equation (2.15)c constitutes a first-order implicit ordinary differential equation. By assuming $\widetilde{H}$ to vary sinusoidally with respect to time

$$\widetilde{H} = \frac{H_p}{H_d}\sin(2\pi n\tilde{t}) \tag{2.20}$$

Equation (2.15)c can be solved using Matlabs implicit 'ODE-lösare *ode15i*'. The initial condition used is $\widetilde{M}(\tilde{t} = 0) = 0$,, indicating that the initial magnetization is zero. The parameter n in equation (2.20) is related to the integration interval as follows

$$\tilde{t} \in \left[0 \; \frac{4n+1}{4n}\right] \tag{2.21}$$

where the end time in this interval corresponds to an initial magnetization (which takes place during the time $0 \leq t \leq \pi/2$) plus n pieces of full hysteresis loops.

Note that M_{an} in equation (2.15)c is singular then $H_e = 0$. However, this singularity can be removed, where it is necessary to

$$\lim_{H_e \to 0} M_{an} = 0 \tag{2.22}$$

$dM_{an}/d\tilde{t}$ in equation (2.17) is also singularity for $H_e = 0$. This singularity can be removed with

$$\lim_{H_e \to 0} \frac{dM_{an}}{d\tilde{t}} = \frac{1}{3}\frac{M_{sd}\widetilde{M}_s}{a_d\tilde{a}}\frac{dH_e}{d\tilde{t}} \tag{2.23}$$

which was calculated with Matlab's symbolic toolbox. The removable singularities in (2.22) and (2.23)are taken into account in the ode function which enters Matlabs ode15i through if statements.

The parameters in the JA model can now be calibrated against the experimental hystereses in Figure 6. This is done by integrating equation (2.15)c for each value of H_p which the experimental data were produced. Different long time intervals are required to achieve a stabilized calculated hysteresis. The smallest hysteresis ($H_p =$ 385 A/m) is fully stabilized after 10 loops ($n = 10$), the middle one ($H_p = 766$ A/m) after 5 loops ($n = 5$), and the largest ($H_p = 11475$ A/m) after 1 loop ($n = 1$). The last calculated loop (corresponding to a stabilized hysteresis) for each is then used to construct a residual vector. The residual vector indicates the difference between experimental and calculated hysteresis, and is defined as

$$\mathbf{R} = [\mathbf{R}_1 \quad \mathbf{R}_2 \quad \mathbf{R}_3] \tag{2.24}$$

where

$$\mathbf{R}_i = [d_{\perp 1} \quad d_{\perp 2} \quad \cdots \quad d_{\perp m_l}] \tag{2.25}$$

Is the residual vector for hysteresis $i = 1,2,3$ in Figure 6. $d_{\perp j}$ indicate the minimum distance measurement point on the experimental hysteresis and the last calculated loop (i.e. fully stabilized hysteresis).

The quantity $d_{\perp j}$ is calculated using a euclidean norm in the space of $\widetilde{H} \times B$. Once again, note that $\mathbf{R}$ contains orthogonal distances between experimental and modeled values in the normalized space of $\widetilde{H} \times B$.

The residual vector **R** is minimized using MATLAB's nonlinear least squares solver Isqnonlin to compute the JA parameters that provide the best fit. The optimized parameters are shown in Table 5 below.

Table 5. Calibrated parameters for the Jiles-Atherton model.

$\boldsymbol{M_s}$ [A/m]	$\boldsymbol{a}$ [A/m]	$\boldsymbol{k_p}$ [A/m]	$\boldsymbol{c_r}$ [-]	$\boldsymbol{\alpha}$ [-]
1.539×10^6	454.6	790.9	0.3434	9.235×10^{-4}

Figure 7 below displays the calculated hysteresis loops for the optimized parameters in Table 5. The black line in the figure represents the BH-relationship computed for the entire time interval (2.21). Note that approximately 7 - 8 loops are required before the smallest hysteresis in Figure 7a stabilizes. The blue line represents the last calculated loop in the time interval(2.21), corresponding to the stabilized hysteresis. The red crosses are experimental data taken from the hysteresis in Figure 6, which were used to create the residual vector in (2.24). Ideally, the blue line should intersect these crosses.

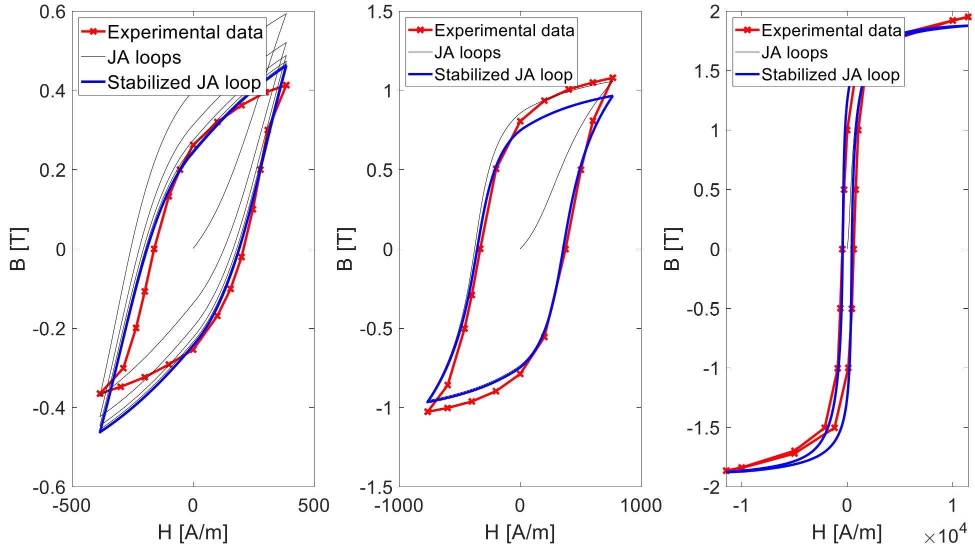

Figure 7. Calculated hysteresis for (a) $\boldsymbol{H_p = 385}$ A/m, $\boldsymbol{n = 10}$, (b) $\boldsymbol{H_p = 766}$ A/m, $\boldsymbol{n = 5}$, (c) $\boldsymbol{H_p = 11475}$ A/m, $\boldsymbol{n = 1}$. The blue line represents the stabilized hysteresis, and the red crosses indicate the experimental data points.

Figure 8 below shows the three calculated stabilized hysteresis loops in a same single figure.

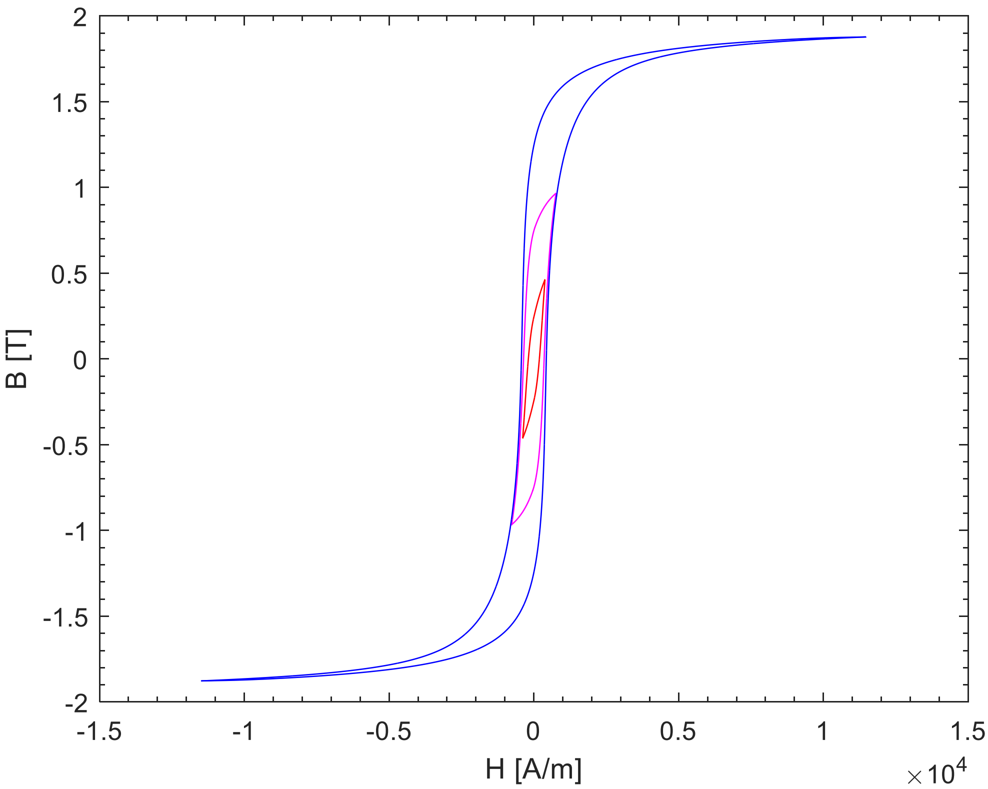

Figure 8. Calculated stabilized hysteresis for $\boldsymbol{H_p = 385}$ A/m, $\boldsymbol{H_p = 766}$ A/m, $\boldsymbol{H_p = 11475}$ A/m.

2.5 FINIT ELEMENT MODELL

Figure 9a shows the computational domain of the axisymmetric pipe model implemented in the program COMSOL [9]. The model is based on two tubes, whose axes lie on the z-axis in the model, which are magnetized by a background field, and then brought together along the z-axis until the distance between the tube ends is the same as the gap distance of the weld. COMSOL's "Magnetic Fields, No Currents" interface has been used here, where equation (2.7) is solved with the finite element method. The lower pipe of the two pipes is located between $z = -L$ and $z = 0$, see Figure 9a, where L is the length of the pipe. The tube is surrounded by an air domain of radius w. Furthermore, the air domain also extends axially beyond the lower end of the tube by a length w, as shown in Figure 9a. The diameter of the tube is D, and its thickness is h. The weld's straight-edge length is u, half of the joint preparation angle is θ, and half of the gap width is d_f. The model exhibits geometric symmetry around $z \equiv d_i$, and the **B** and **H** fields are antisymmetric around $z \equiv d_i$. This enables modeling only one of the two pipes (under the condition that magnetization is such that **B** and **H** are antisymmetric). Figure 9a also depicts the boundary conditions (2.10) and (2.11). Figure 9b-f display the mesh at different levels of zooming in. The smallest element size is determined by the parameter m_p.

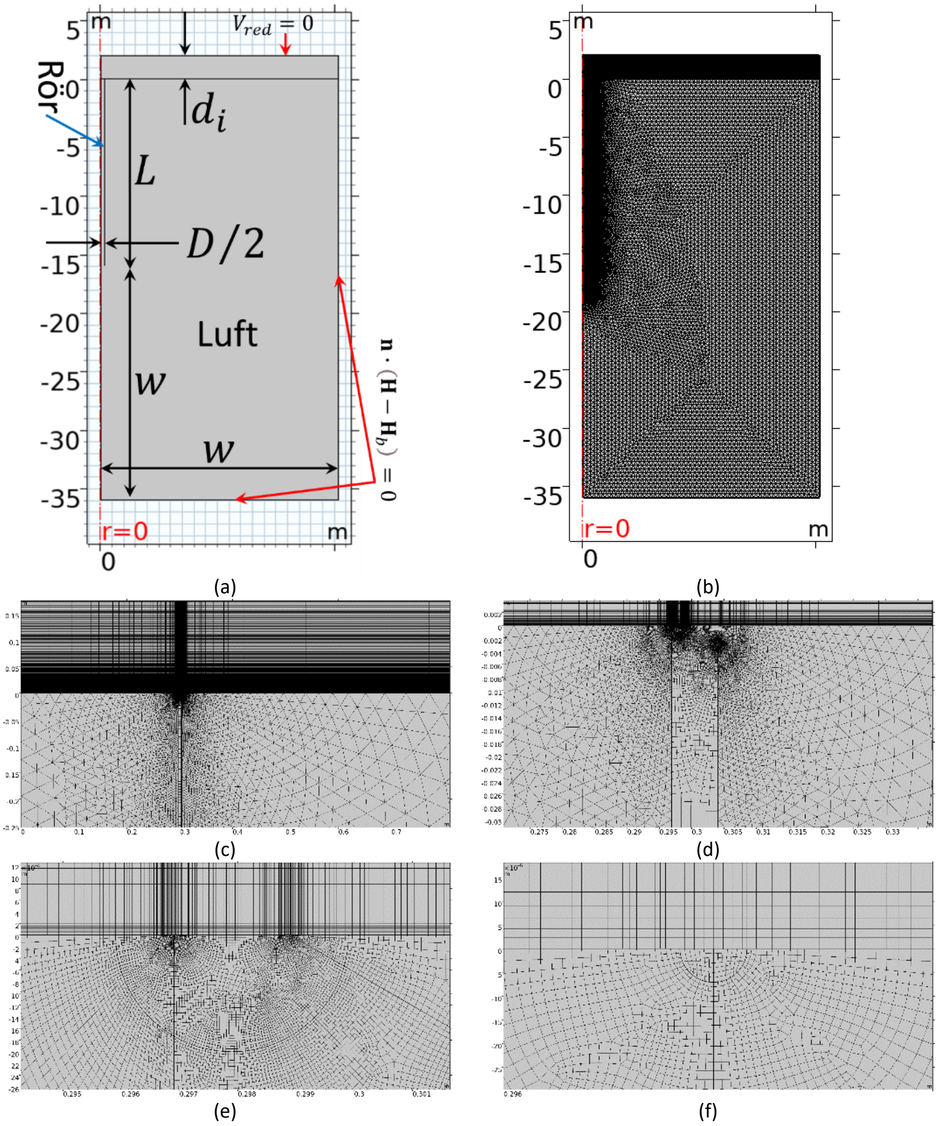

Figure 9. (a) Computational domain and boundary conditions, (b)-(f) different levels of mesh zooming.

All calculations in this report are applied to DN600 pipes (with dimensions and joint geometry specified in Table 6 below) unless otherwise stated.

Table 6. Pipe dimensions and joint geometry for DN600 pipes are as follows.

D	L	h	u	θ
608 mm	16 m	7.1 mm	2 mm	30°

2.5.1 Magnetization

The model is magnetized with the background field described in equation (2.12) during the time interval $0 \leq t \leq 1$ s. At time zero, the background field is zero; at time 0.5 s, the maximum value $B_{bp} = H_{bp}/\mu_0$ is reached; and at time 1 s, the background field returns to zero. The background field is assumed to vary slowly enough to satisfy the assumption of magnetostatics. For time stepping, a Back

Differentiation Formula (BDF) method is used, where the time step Δt is determined adaptively. The time step is considered converged when a computed residual falls below a given tolerance R_{tol}.

During magnetization ($0 \leq t \leq 1$), the distance $2d_i$ (which denotes the distance between two opposite pipe ends, as shown in Figure 9a) remains constant. d_i is chosen to be sufficiently large so that the magnetic field from one pipe does not significantly influence the magnetic field in the other pipe during the magnetization phase.

2.5.2 Merging of Two Magnetized Pipes

After the pipes have been magnetized, they are brought together to a gap distance of $2d_f$. This is done by continuously deforming the air domain $\Omega_i = [0\ w] \times [0\ d_i]$ to $\Omega_f = [0\ w] \times [0\ d_f]$ during the time interval $1 < t \leq 2$ s. The deformation is carried out using an Arbitrary Lagrangian-Eulerian (ALE) formulation applied to the elements in Ω_i. These elements are vertically deformed according to the prescribed deformation.

$$\Delta Z = -Z_g + f \cdot g \tag{2.26}$$

where

$$\begin{cases} g = \left(1 - \dfrac{Z_g}{f}\right) \mathrm{int2}(t) + \dfrac{Z_g}{f} \\ f = \dfrac{2Z_g d_f}{N f_d \left(-1 + 2m_p - \frac{f_p}{2} + \sqrt{\frac{f_p^2}{4} + \frac{2Z_g(N-1)}{R_e m_p - m_p}}\right)} \end{cases} \tag{2.27}$$

where

$$\begin{cases} f_p = \dfrac{2(N-1)}{(R_e - 1)} - 1 \\ f_d = \dfrac{m_p(R_e - 1)}{(N-1)} \end{cases} \tag{2.28}$$

where

$$R_e = \frac{2d_i}{N m_p} - 1 \tag{2.29}$$

Here, Z_g represents the vertical component in the coordinate system of the model's geometry, and N is the number of element rows in the vertical direction that Ω_i is divided into . The element partitioning of Ω_i in the vertical direction is determined by an arithmetic sequence where the ratio between the longest and shortest vertical element lengths is given by R_e. $\mathrm{int2}(t)$ is a function that varies from 0 to 1 in the time interval $1 < t \leq 2$ s according to Figure 10 below. ΔZ in (2.26) has the property that the elements in the air gap will have an arithmetic distribution in the vertical direction for $0 \leq t \leq 1$, where the smallest element has the size m_p. This leads to a "continuous" variation of element size in the z-direction at $z = 0$ (see Figure 9f), which improves convergence. Furthermore, ΔZ in (2.26) has the property that all elements in Ω_f will have the same size in the vertical direction when $t = 2$ s,, which also enhances convergence by avoiding severely flattened elements when Ω_i is deformed to Ω_f.

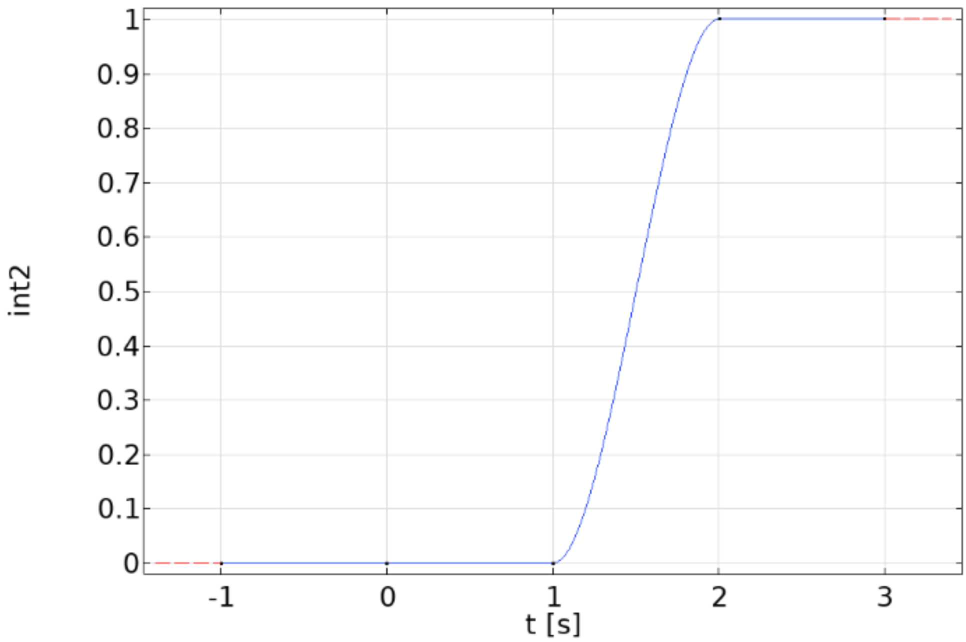

Figure 10. Function of $\mathbf{int2}(\boldsymbol{t})$.

2.5.3 Convergence Study

All calculations in this work have been performed using the model parameter values specified in Table 7 below (unless stated otherwise). These parameter values (except for the gap width $2d_f$ and the background field B_{bp}) have been chosen such that the magnetic field in the weld gap has a minimal dependence on their magnitude. For instance, the radius of the air domain, w, has been selected to be large enough that an increase in its magnitude only results in a very small change in the magnetic field within the weld gap.

Table 7. Model Parameters.

Δt	R_{tol}	m_p	w	d_i	d_f	B_{bp}
Adaptive Time Step Control	10^{-3}	0.01 mm	20 m	2 m	1 mm	2 G

To study the sensitivity of the parameter values in Table 7, the relative error is defined as

$$\delta = \frac{\|\mathbf{B}\| - \|\mathbf{B}\|_{ref}}{\|\mathbf{B}\|_{ref}} \times 100\% \tag{2.30}$$

where $\|\mathbf{B}\|_{ref}$ is computed based on the values in Table 7, while $\|\mathbf{B}\|$ is calculated with a change in one of the parameter values in Table 7.

In Table 8 below, δ has been calculated for several different variations of the model parameters. This was done at $t = 2$ s and at eight points located at the center of the weld gap as shown in Figure 11 below.

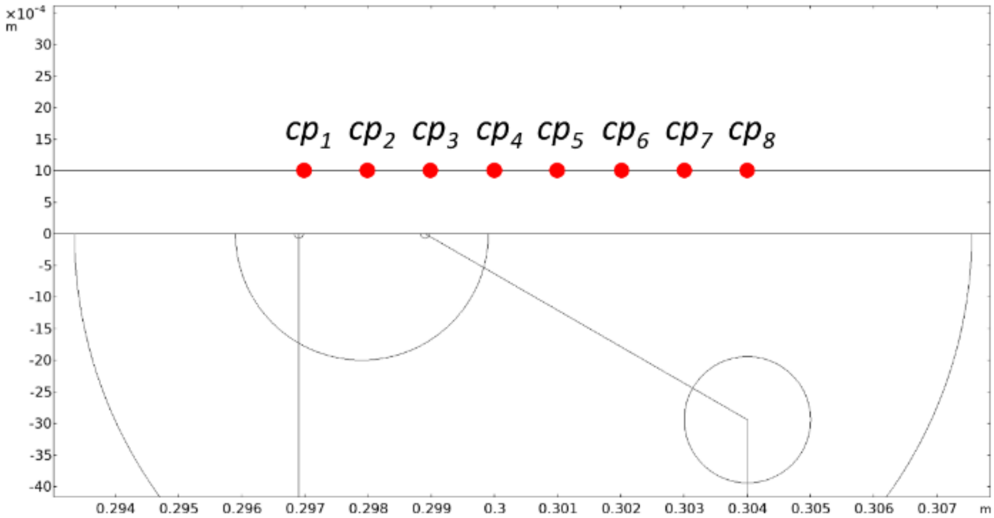

Figure 11. Evaluation points for the $\boldsymbol{\delta}$.

From the second and third columns in Table 8 , it can be observed that when fixed time steps 0.01 and 0.001 s are used, the magnetic field changes by only a few tenths of a percent compared to the adaptive time stepping. Hence, the adaptive time stepping is considered to yield a converged result with respect to the time step size. Furthermore, from the fourth column, it can be seen that changing the tolerance for the residual (which indicates when a time step is considered converged) from 10^{-3} to 10^{-4} results in only about a 0.5% change in the magnetic field at the center of the weld gap. Therefore, $R_{tol} = 10^{-3}$ is considered a converged value. From the fifth column, it is evident that when the element size is halved, the magnetic field changes by only about 0.05%. When the radius of the air domain increases from 20 to 30 m, the magnetic field changes by only a few percent, as seen in the sixth column. Finally, when the distance between the pipes is $2d_i = 6$ m instead of 4 m during magnetization ($0 \leq t \leq 1$), the magnetic field changes by approximately 0.5%.

Table 8. δ- values for different variations of model parameters, calculated in the points indicated in Figure 11.

	$\Delta t =$ 0.01 s	$\Delta t =$ 0.001 s	R_{tol} $= 10^{-4}$	$m_p =$ 0.005 mm	$w =$ 30 m	$d_i = 3$ m
cp_1	0.18	0.38	0.49	0.039	1.0	-0.41
cp_2	0.18	0.38	0.49	0.044	1.0	-0.41
cp_3	0.18	0.38	0.50	0.046	1.0	-0.41
cp_4	0.20	0.43	0.55	0.050	1.0	-0.39
cp_5	0.20	0.44	0.56	0.061	1.0	-0.39
cp_6	0.20	0.44	0.57	0.072	1.0	-0.39
cp_7	0.20	0.45	0.57	0.060	1.1	-0.40
cp_8	0.20	0.45	0.57	0.068	1.1	-0.40

3 Result from numerical simulation

In this chapter, the numerical model developed in the previous chapter is applied to study the magnetic field in and around magnetized district heating pipes. First, magnetic field lines are calculated to illustrate the magnetic field around two magnetized tubes. Then the magnitude of the background field required to magnetize a district heating tube to such a level that arc instability/arc deflection problems may occur is determined. After this, the influence of the magnetic field of the earth and power lines on the residual magnetism in a district heating pipe is investigated. Finally, the influence of the dimensions of the pipes, and the geometry of the gap, on the magnetic field around the welding gap was studied. This is to investigate whether, for example, it is easier to magnetize a large tube than a small tube to such a level that, for example, arc deflection can occur.

For all the calculations below, the pipe dimensions in Table 6, and the model parameters in Table 7, have been used unless it is specified.

3.1 MAGNETIC FIELD LINE

Figure 12 shows the field line of the **B**-field for two DN600 pipes at $t = 1$ s, which have been magnetized with $B_{bp} = 2$ G. The density between the field lines depends on the field strength, where high density indicates high field strength. The left part of the figure has been achieved by mirroring the **B**-field antisymmetrically in $z = d_i$.

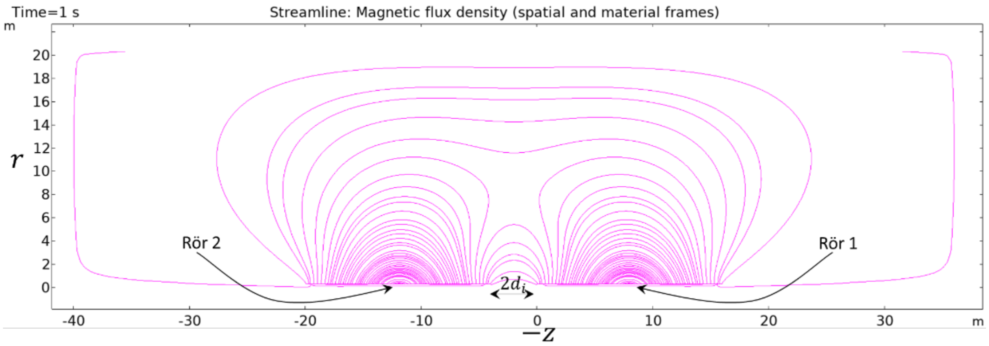

Figure 12. Field lines of the **B**-field with $t = 1$ s and $B_{bp} = 2$ G.

Figure 13 shows the field lines in more detail at the pipe end $z = 0$. The figure also shows the contour plot of the field of $\|\mathbf{B}\|$.

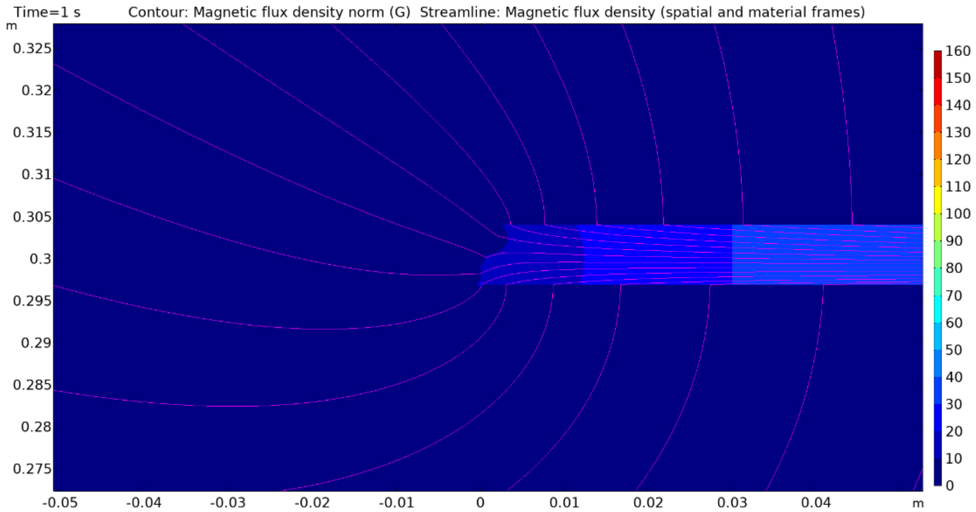

Figure 13. The field of $\mathbf{B}$ and contour plot of $||\mathbf{B}||$ with $\boldsymbol{t} = \mathbf{1}$ s and $\boldsymbol{B_{bp}} = \mathbf{2}$ G.

Figure 14 shows the field lines when $t = 2$ s and the tubes have been brought together to the final gap distance, where $2d_f = 2$ mm. The figure also shows a contour plot for the $||\mathbf{B}||$-field. From the figure, it can be seen that the magnetic field is greatest at the corners of the right edge.

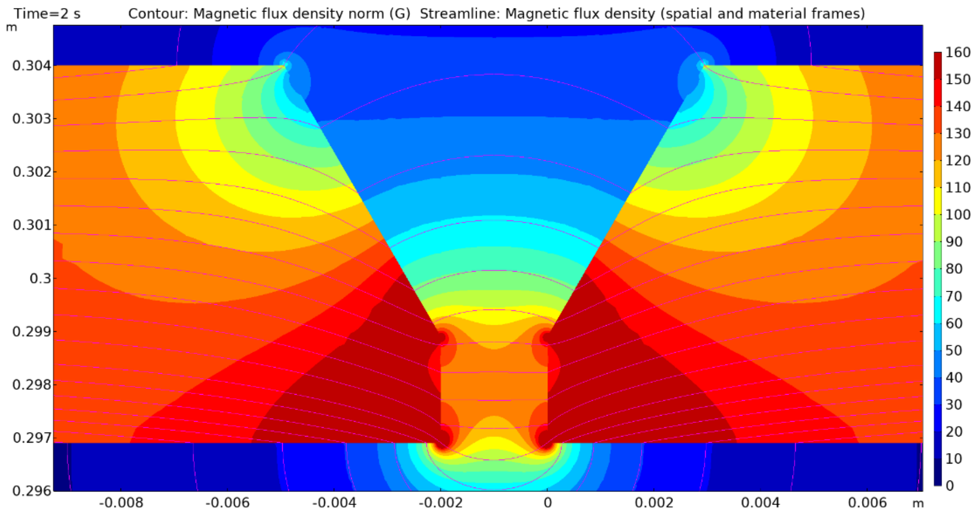

Figure 14. The field of B and contour plot of $\|$ B $\|$ with $\boldsymbol{t} = \mathbf{2}$ s and $\boldsymbol{B_{bp}} = \mathbf{2}$ G.

3.2 ARC DEFLECTION

In chapter 1.4, it is stated that arc deflection for manual arc welding occurs when the magnetization reaches approximately 40 G. From Figure 15, it can be seen that an approximately 10 mm large area, approximately centered around the root gap, occurs where $||\mathbf{B}|| > 40$ G when the DN600 pipe is magnetized with the background field $B_{bp} = 2$ G.

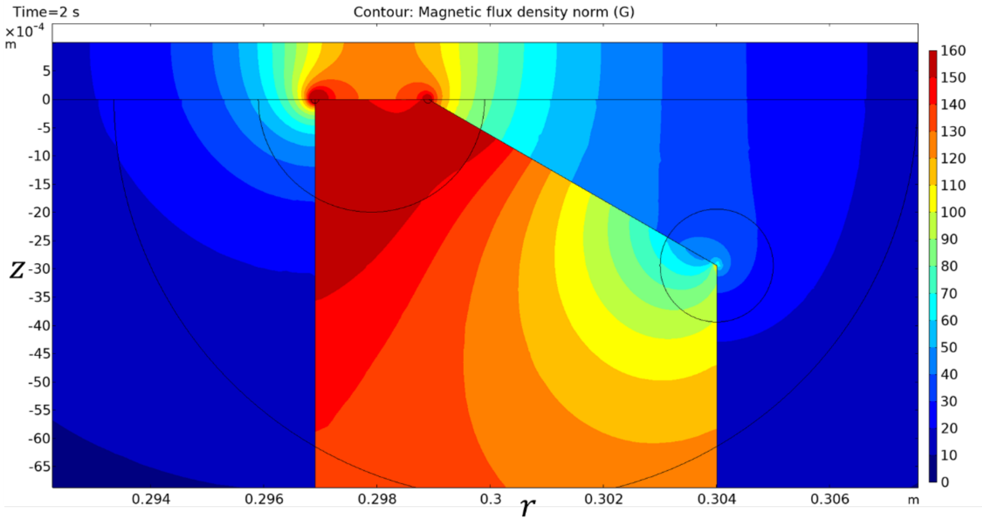

Figure 15. $\|\mathbf{B}\|$-field with $\boldsymbol{t} = \mathbf{2}$ s and $\boldsymbol{B_{bp}} = \mathbf{2}$ G.

In the area where $\|\mathbf{B}\| > 40$ G, the B field is dominated by the z-component, which can be seen by comparing Figure 16a and b. Here it can be seen that the area where $B_z > 40$ G (right Figure) is approximately the same size as the area where $\|\mathbf{B}\| > 40$ G (left Figure). This means that only the axial component of the magnetic field needs to be measured when investigating whether there is a risk of arc deflection, which simplifies the measurement.

.

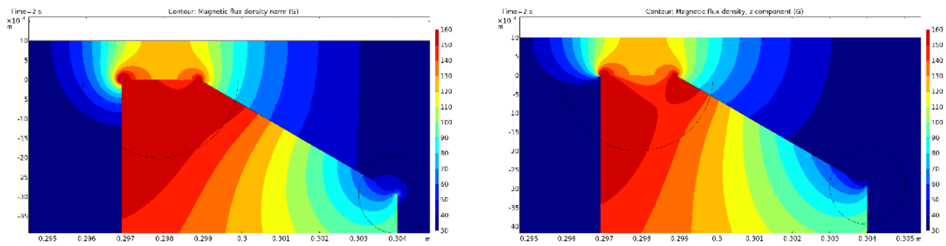

(a) (b)

Figure 16. (a) $\|\mathbf{B}\|$-field and (b) $\boldsymbol{B_z}$ with $\boldsymbol{t} = \mathbf{2}$ s with $\boldsymbol{B_{bp}} = \mathbf{2}$ G.

Figure 17 shows the strong strengthening of the magnetic field in the weld gap that occurs when the tubes are brought together to the gap distance $2d_f = 2$ mm after they have been magnetized with the background field $B_{bp} = 2$ G. The left figure shows the area where B_z>8 G and t=1 s, i.e. just after the magnetization and just before when the tubes start to be brought together. The right Figure shows the area where $B_z > 40$ G and $t = 2$ s, i.e. when the gap distance is $2d_f = 2$ mm. This amplification is important to take into account when magnetic field measurements are made to detect the risk of arc deflection. If the pipes are not joined together, for example if they lie on a stack, then it is not the threshold value of 40 G that you should look for. Instead, one should look for values around $|B_z| > 8$ G. Here, in the worst case, if one pipe end has $B_z > 8$ G (magnetic north pole) and the other pipe end has $B_z < -8$ G (magnetic south pole), the area where $B_z > 40$ G when the tubes have been brought together be equal to or greater than that in Figure 17b.

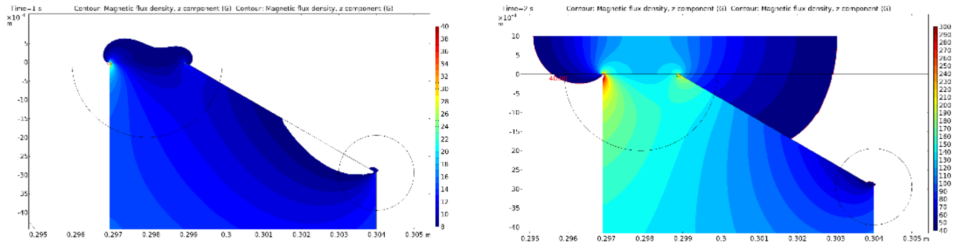

(a) (b)

Figure 17. (a) $\boldsymbol{B_z > 8}$ G with $\boldsymbol{t = 1}$ s, (b) $\boldsymbol{B_z > 40}$ G with $\boldsymbol{t = 2}$ s. $\boldsymbol{B_{bp} = 2}$ G.

3.3 ARC INSTABILITY

Arc instability was stated in chapter 1.4 to occur when $\|\mathbf{B}\| > 20$ G. Figure 18b shows that an approximately 10 mm area where $B_z > 20$ G occurs with the magnetized background field $B_{bp} = 1.5$ G. Figure 18a shows the area where $B_z > 4$ G at $t = 1$ s for the magnetization $B_{bp} = 1.5$ G. From this figure it can be seen that a magnetic field value would show approximately 4 – 5 G at the right edge before the joining.

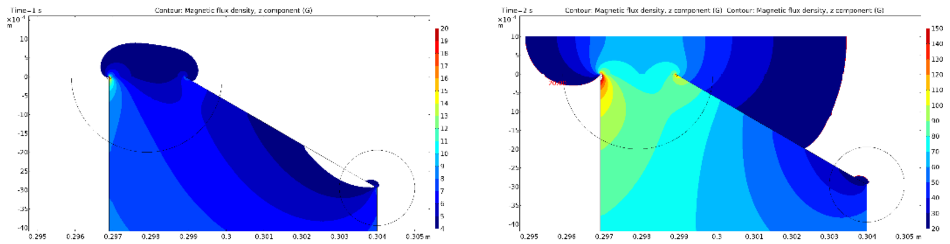

(a) (b)

Figure 18. (a) $\boldsymbol{B_z > 4}$ G with $\boldsymbol{t = 1}$ s, (b) $\boldsymbol{B_z > 20}$ G with $\boldsymbol{t = 2}$ s. $\boldsymbol{B_{bp} = 1.5}$ G.

3.4 THE EARTH'S MAGNETIC FIELD

It has been discussed whether the Earth's magnetic field can give rise to a residual magnetism that can lead to arc instability. To investigate this, our model was run with $B_{bp} = 0.15$ G, which corresponds to the horizontal component of the earth's magnetic field in Sweden [14], see Figure 19.

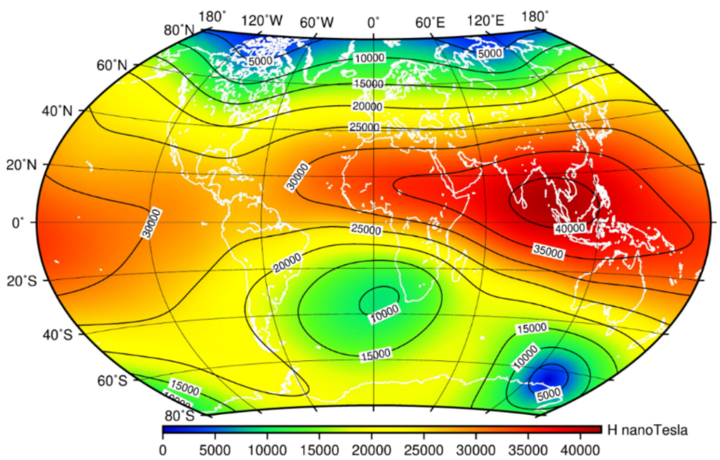

Figure 19. Horizontal component of the Earth's magnetic field [14].

Figure 20 shows the calculated ||**B**||-field at t=2 s for $B_{bp} = 0.15$ G. According to the magnetization cycle, described in chapter 2.5.1, the magnetization in Figure 20 can be thought to occur when the tube is first oriented perpendicular to one of the Earth's meridian lines, to then be rotated so that it lines up with the meridian line, to finally be rotated back to the original position. As can be seen from the figure, this results in a magnetization of less than 1 G, and there is therefore no risk of arc instability.

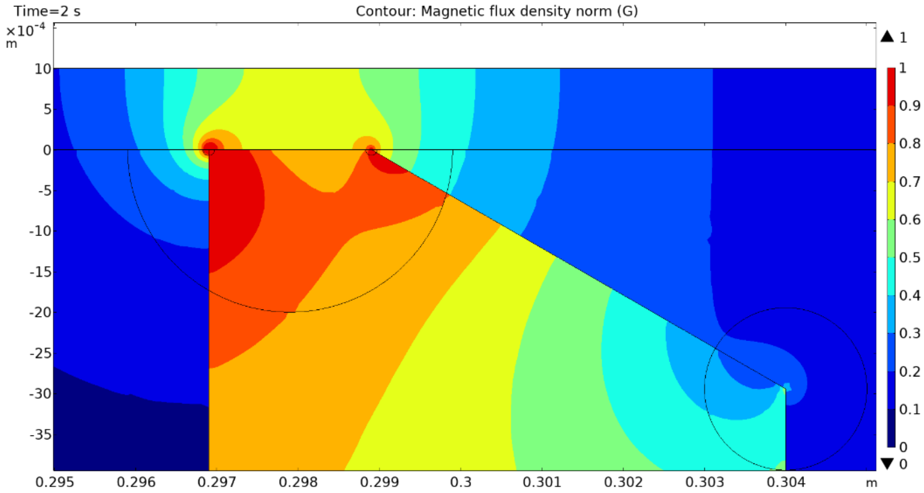

Figure 20. ‖ B ‖ -field with $\boldsymbol{t = 2}$ s, magnetized from the Earth's magnet field ($\boldsymbol{B_{bp} = 0.15}$ G).

A much stronger magnetization occurs if the tube is not turned back to its original position, but remains tangential to the meridian. Such a magnetization can be achieved by replacing the function $\mathrm{int1}(t)$ in Figure 4a, and equation (2.12) with $\mathrm{int1}(t)$ in Figure 21.

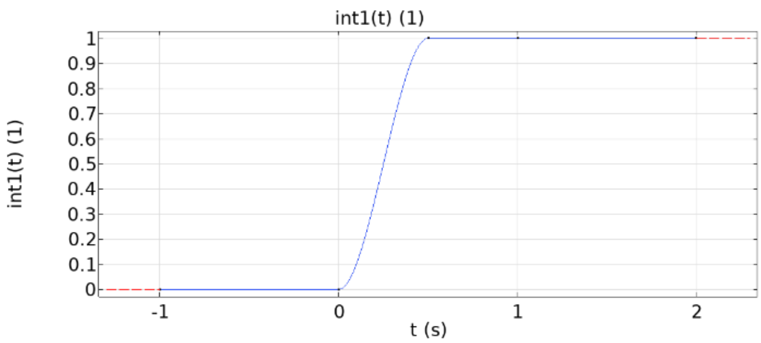

Figure 21. Modified $\mathbf{int1}(\boldsymbol{t})$ function.

Figure 22 shows the calculated ||**B**|| field for t=1 s and t=2 s, with $B_{bp} = 0.15$ G and $\mathrm{int1}(t)$ according to Figure 21. The magnetic field is significantly stronger now that the tube remains aligned with the meridian (compare Figure 20 and Figure 22b). A 5 mm wide area around the weld gap has a magnetization greater than 20 G, which may pose a risk of arc instability.

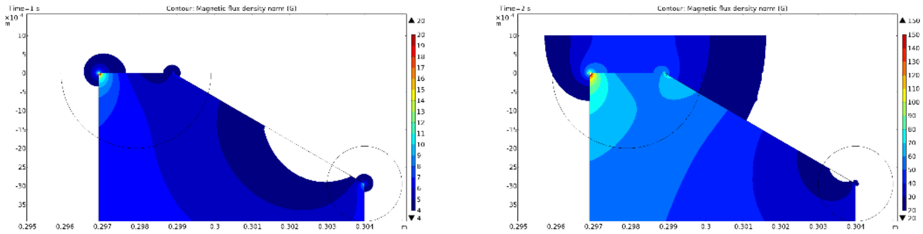

(a) (b)

Figure 22. (a) $\|\mathbf{B}\| > 4$ G with $t = 1$ s, (b) $\|\mathbf{B}\| > 20$ G with $t = 2$ s.

To understand why the magnetization is much stronger when the pipe remains tangential to the meridian, as compared to when it is rotated back to the perpendicular position, we examine the BH-curve in Figure 23a.. This BH curve has been generated from the JA model in equation (2.15) by increasing the H-field from zero to $H = H_{bp} = B_{bp}/\mu_0 = 12$ A/m and then returning it to zero. After this cycle, a magnetization of approximately 3 G is observed (see the B-value for $H = 0$ in Figure 23a). This cycle corresponds to the magnetization cycle in Figure 20.

Alternatively, if the H-field increased to $H = H_{bp}$ and locked there, a magnetization of approximately 90 G is achieved. This is 30 times higher than in the previous case. This magnetization cycle corresponds to Figure 22 and explains why the magnetization becomes much more powerful in this scenario. However, it should be noted that the JA model is not calibrated for these small H-fields and may therefore introduce significant errors.

Figure 23b displays the initial magnetization curve when H goes from zero to 2 kA/m. This curve has a steep slope for small H-values, which may not be entirely accurate. As a result, the magnetic fields in Figure 22 may be overestimated.

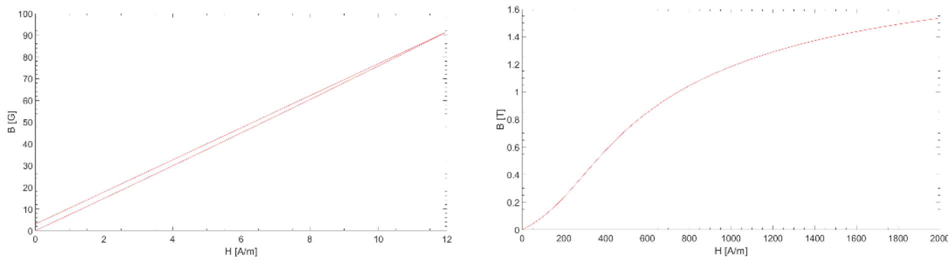

(a) (b)

Figure 23. (a) The BH relationship calculated using the JA-model. The lower curve shows the initial magnetization for $0 < H < H_{bp} = 12$ A/m. The upper curve presenting when $H = 0$. (b) The BH relationship calculated using the JA-model for $0 < H < 2$ kA/m.

3.5 THE ELECTRICAL POWER LINE

It has been speculated whether high voltage electrical lines can give rise to residual magnetism when the steel pipes are transported under them. This is not something that can be calculated directly with our magnetostatic model because the magnetic field from a high-voltage line is time-varying. In addition, there is a time-varying electric field around the power line that is connected to the magnetic field via Maxwell's equations, which is also not taken into account in our magnetostatic model. However, to roughly estimate the influence of a power line on the residual magnetism in a steel pipe, we run the measured magnetic field from the line as a uniform background field in our model. Measurements have shown that in the month of February, when power consumption is at its highest, the magnetic field under 400 kV power lines (which are the largest power lines in Sweden) is about 0.1 – 0.2 G, 1.5 m above the ground [15]. When the model is run with $B_{bp} = 0.2$ G, the magnetization is obtained in Figure 24. The maximum magnetic field in the gap amounts to approximately 1.5 G, well below the limit for arc instability. Note that this is a rough estimate as no account has been taken of the time variations of the electric and magnetic fields. But it is possible that this time variation gives a lower magnetization because the fields will have time to change direction several times before the pipe has time to be transported under the power line.

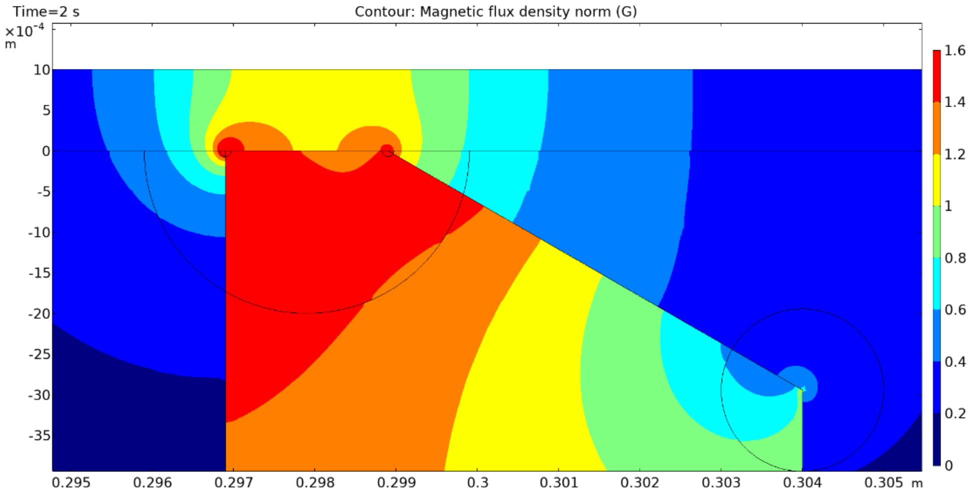

Figure 24. $\|\mathbf{B}\|$-field with $t = 2$ s, magnetized from the power line ($B_{bp} = 0.20$ G).

3.6 PIPE DIMENSIONS AND GEOMETRY GAP

In this section, the influence of tube dimensions and gap in geometry on the strength of the magnetic field in the weld gap is studied. As a comparison reference, the pipe dimension in Table 6 and the model data in Table 7 are used as before.

3.6.1 Pipe length

Figure 25 shows the $\|\mathbf{B}\|$-field at the weld gap for four DN600 pipes with the lengths: L=16 (reference), 1, 10 and 20 m, all magnetized with the same background field ($B_{bp} = 2$ G). From the figure it can be seen that the shortest pipe has a markedly lower magnetization than the other pipes. The area where $\|\mathbf{B}\| > 40$ G is approximately the same for pipe lengths 10, 16 and 20 m.

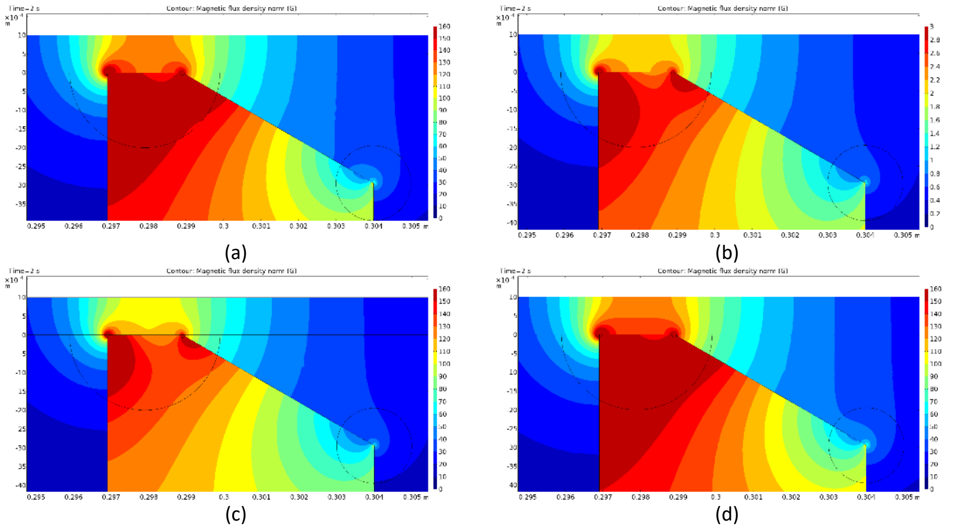

Figure 25. ||**B**||-field for pipe length L: a) L = 16 m (reference), b) L = 1 m, c) L = 10 m, and d) L = 20 m. with t = 2 s.

Figure 26 shows the value of the ||**B**||- field at t = 2 s, in points cp4 and cp5 (see Figure 11) as a function of the pipe length L. It's worth noting the interesting observation that the||**B**||- field becomes constant after approximately L = 15 m.

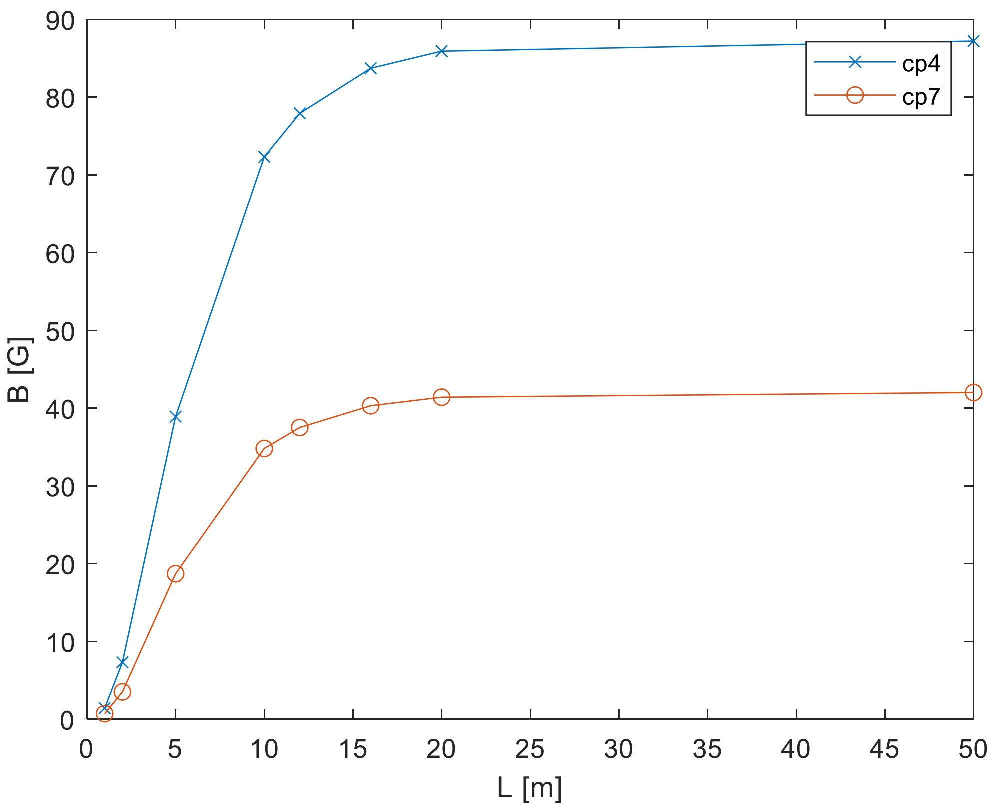

Figure 26. The value of ||**B**||-field in points of cp4 and cp5 as a function of pipe length.

3.6.2 Pipe diameter

In Figure 27, the ‖**B**‖- field at the weld gap is shown for four DN600 pipes with the following diameters: D=608 (reference), 100, 200, and 750 mm. All of these pipes have been magnetized with the same background field ($B_{bp} = 2$ G). From the figure, it can be observed that the region where $\|\mathbf{B}\| > 40$ G is approximately the same size for all the pipes with different diameters. The magnetic field at the weld edge is also roughly the same for the different pipes. From this, one can conclude that the magnetic field in the weld gap is minimally affected by the pipe diameter.

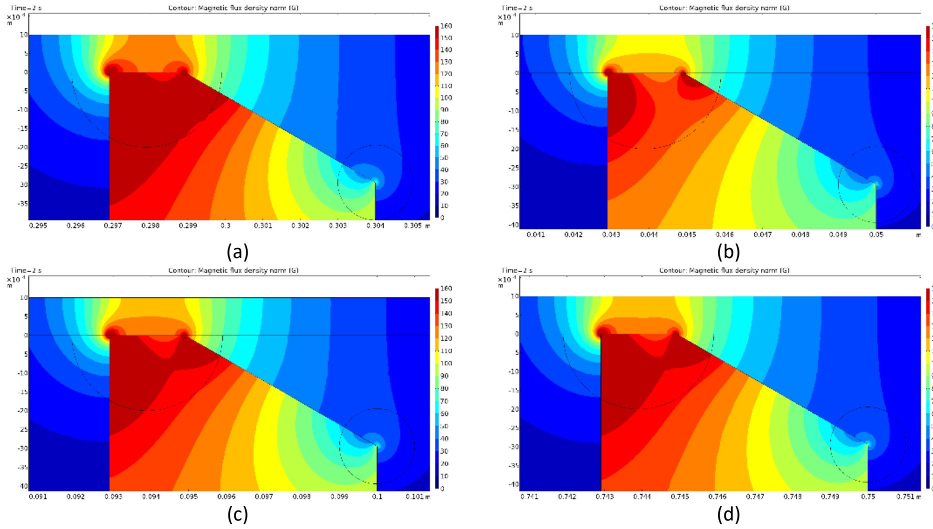

Figure 27. ‖**B**‖-field of pipe diameter : a) D = 608 mm (reference), b) D = 100 mm, c) D = 200 m, and d) D = 750 m. t = 2 s.

3.6.3 Straight edge

In Figure 28, the ‖**B**‖- field at the weld gap is shown for four DN600 pipes with straight edges: $u = 2$ (reference), 0.2, 1 and 4 mm, all magnetized with the same background field ($B_{bp} = 2$ G). From the figure it can be seen that the area where $\|\mathbf{B}\| > 40$ G is approximately 40% larger for the pipe with $u = 4$ mm than for the pipe with $u = 0.2$ mm. However, the magnetic field is slightly stronger at the ends (corners) of the right edges when $u = 0.2$ mm compared to $u = 4$ mm.

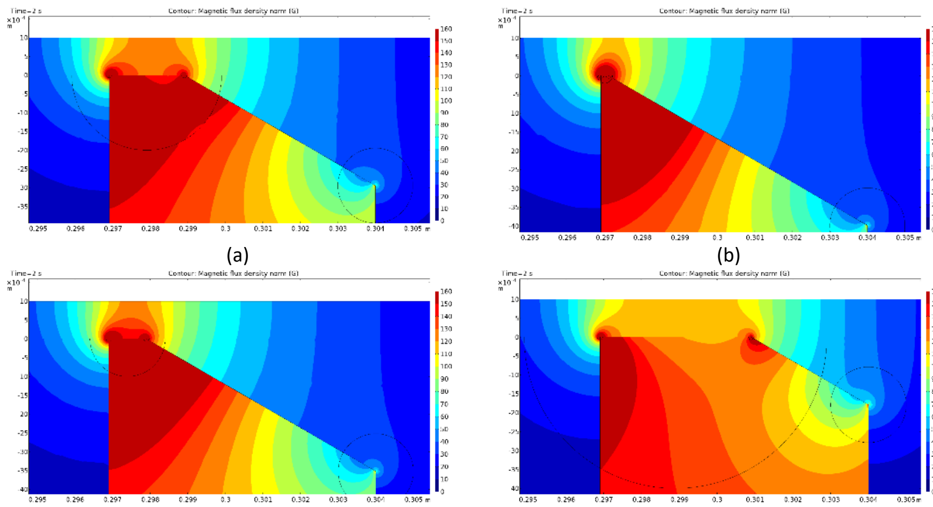

Energiforsk

(c) (d)

Figure 28. ||**B**||-field of straight edge: a) u = 2 mm (reference), b) u = 0.2 mm, c) u = 1 mm, and d) u = 4 mm. t = 2 s.

3.6.4 Pipe thickness

In Figure 29, the ||**B**||- field at the weld gap is shown for four DN600 pipes with material thicknesses: $h = 7.1$ (reference), 4, 5 and 15 mm, all magnetized with the same background field ($B_{bp} = 2$ G). From the figure it can be seen that the area where ||**B**|| > 40 G is strongly dependent on the material thickness. This area is approximately 60% larger for $h = 15$ mm compared to $h = 4$ mm. The magnetic field also increases in strength at the right edge as the material thickness increases.

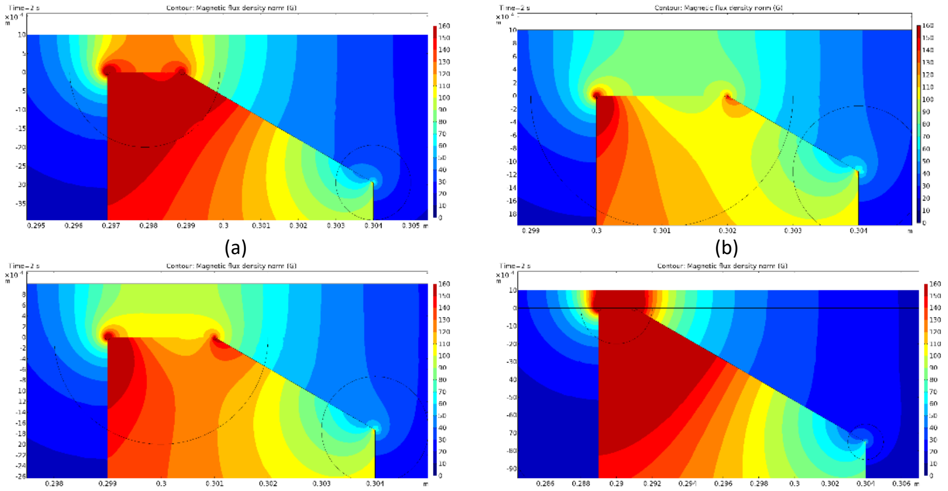

(a) (b) (c) (d)

Figure 29. ||**B**||-field pipe thickness: a) h = 7.1 mm (reference), b) h = 4 mm, c) h = 5 mm, and d) h = 15 mm. **t = 2 s.**

3.6.5 Joint bevel angle

In Figure 30, the ||**B**||-field at the weld gap is shown for four DN600 pipes with joint angles: $2\theta = 60°$ (reference), 30°, 40° and 120°, all magnetized with the same background field ($B_{bp} = 2$ G). From the figure it can be seen that the area where ||**B**|| > 40 G is reduced as θ is increased. For example, the size of this area is reduced by approximately 30% when θ is increased from 15° to 60°. However, the strength of the magnetic field at the right edges increases slightly when θ is increased.

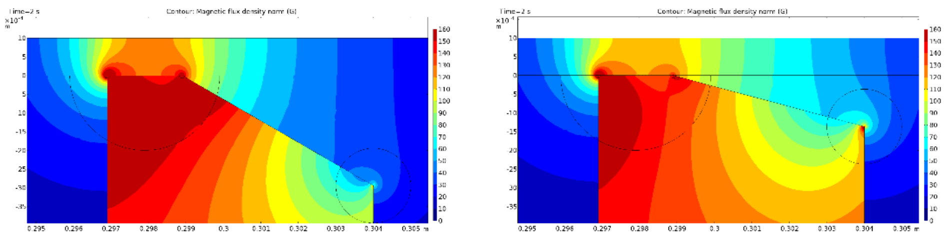

(a) (b)

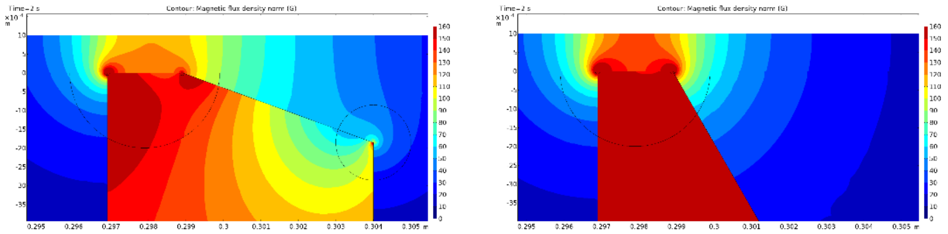

(c) (d)

Figure 30. ||**B**||-field bevel angel: a) $2\theta = 60°$ (reference), b) $2\theta = 30°$, c) $2\theta = 40°$, and d) $2\theta = 120°$. t = 2 s.

3.6.6 Gap width

In Figure 30, the ||**B**||- field at the welding gap is shown for four DN600 pipes with the gap widths: $2d_f = 2$ (reference), 1, 3 and 4 mm, all magnetized with the same background field ($B_{bp} = 2$ G). From the figure it can be seen that the ||**B**||-field is greatly strengthened in the root gap when the gap width is reduced. However, the size of the area where $\|\mathbf{B}\| > 40$ G decreases slightly when the gap width is reduced.

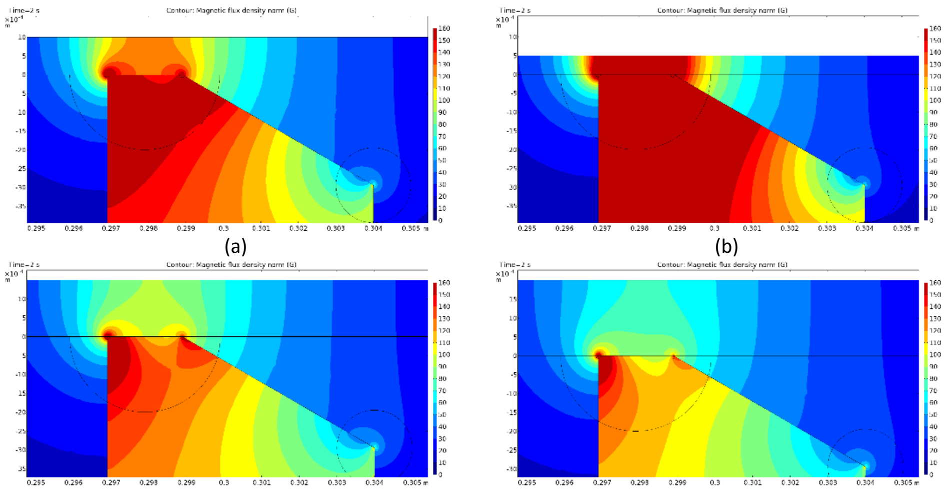

(a) (b) (c) (d)

Figure 31. ||**B**||-field for gap width: a) $2d_f$ = 2 mm (reference), b) $2d_f$ = 1 mm, c) $2d_f$ = 3 mm, and d) $2d_f$ = 4 mm. t = 2 s.

3.7 SUMMARY OF RESULTS

The most important results from the numerical calculations in this chapter are summarized here.

- Simulations show that an external magnetic field with a strength of 2 Gauss or higher can magnetize a district heating pipe to a level where arc deflection may occur.
- Simulations reveal that the magnetic field in the weld gap between two magnetized pipes can be many times greater than at the two opposing pipe ends before the pipes are brought together to form the weld gap. This is crucial to consider when assessing the risk of arc deflection in isolated pipes, as the measured value can significantly increase when the pipe is joined with another magnetized pipe.

- A magnetic field is a vector field with three components. The strength of the magnetic field is often represented by its Euclidean norm, which requires knowing all three components of the field to be determined. Therefore, three measurements are needed to determine the field strength at a given point, which can be challenging. However, numerical simulations show that the strength of the magnetic field in the weld gap and at the straight edges of the pipes, where arc deflection occurs, is well represented by the magnitude of the axial component of the magnetic field. This means that only one measurement is required to determine the field strength at a given point in this area, simplifying the measurement procedure significantly when assessing arc deflection.
- Numerical calculations indicate that the Earth's magnetic field and power lines' magnetic fields have a minimal impact on the residual magnetism in district heating pipes. That magnetic fields are too weak to cause arc deflection in district heating pipes.
- Numerical simulations demonstrate that the magnetic field in the weld gap is moderately dependent on pipe diameter, straight edge length, and joint bevel angle. However, it is strongly dependent on material thickness and gap width. It is also highly dependent on pipe length when the length is less than 10 m; beyond that, the dependence diminishes significantly.

4 Experimental equipment and experimental set-up

This chapter presents a robust method for measuring the magnetic field at pipe ends and in weld gaps between district heating pipes. An experimental set-up to investigate the risk of arc deflection is also reported.

4.1 MEASUREMENT OF MAGNETIC FIELDS

The magnetic field meter MAGMETER MF300H+, manufactured by Diverse Technologies & Systems Ltd [16], was used in this work to perform magnetic field measurements. This magnetic field meter has a 2 mm wide stainless measuring probe that measures the component of the $\mathbf{B}$ -field perpendicular to the measuring probe. This allows the meter to be used to measure the B_z-component in the weld gap of 2mm or wider.

Figure 32. Magnetic field meter MAGMETER MF300H+ [16].

From the previous chapter, significant gradients in the magnetic field were observed at a pipe's end. This means that when measuring the magnetic field at a pipe's end, the measurement value is strongly dependent on the probe's orientation and position. To ensure better control over the probe's orientation and position, a measurement stand was developed in which the probe can be mounted, as shown in Figure 33.

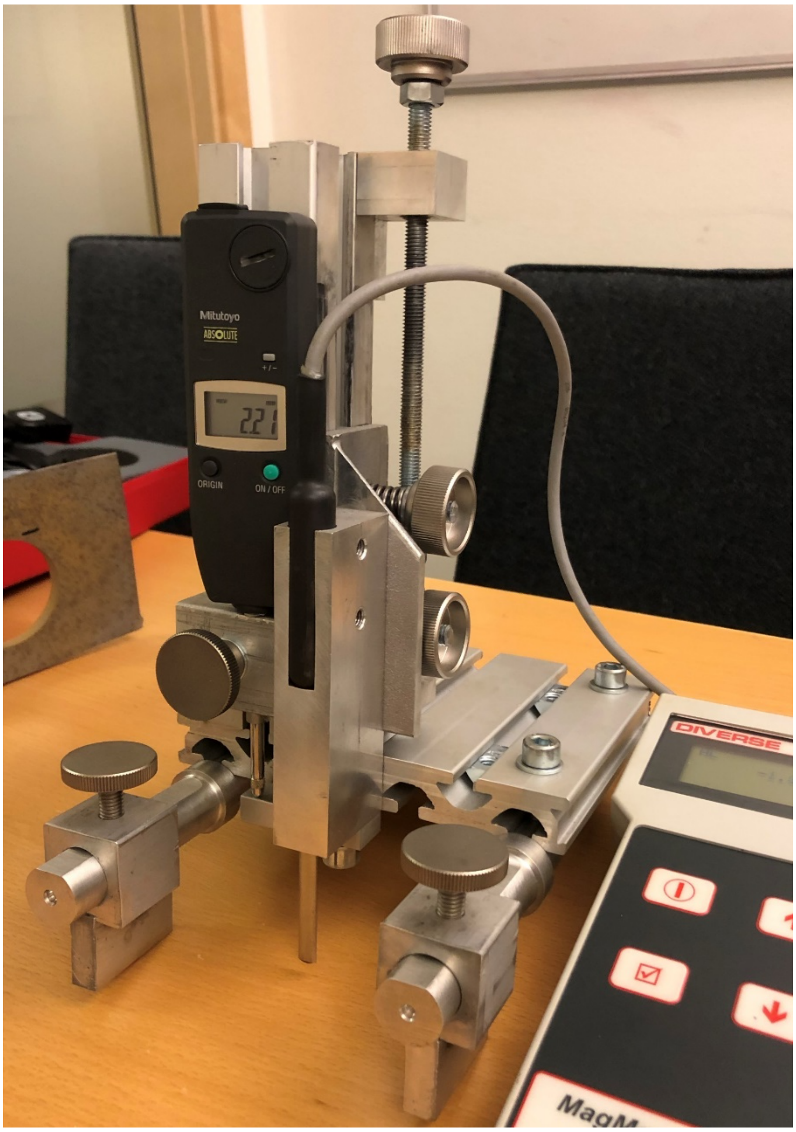

Figure 33. Stand of measurement.

With this measuring stand, both B_z (the axial component) and B_θ (the annular component) can be measured with high accuracy for a free pipe end, and the B_z component in a weld gap. When measurements are carried out on a free pipe end, the measuring stand can be placed both outside and inside the pipe (if the pipe diameter is large enough). Two stops enable quick positioning of the measuring stand in the axial direction of the pipe, and four supports ensure that the measuring probe is oriented in the radial direction of the pipe. By turning the measuring probe 90° in the holder of the measuring stand, you can choose to measure the B_z or B_θ component. With the help of a screw, the measuring stand can move the measuring probe in the radial direction with an accuracy of one hundredth of a mm.

Figure 34. A measured probe is positioned on the straight edge of a DN600 pipe to measure the $\boldsymbol{B_z}$-components. By rotating the probe $\mathbf{90}$° around its axis, the $\boldsymbol{B_\theta}$-components can be measured. The measurement stand that holds the probe is located inside the pipe.

4.2 EXPERIMENTAL SETUP FOR INVESTIGATING ARC INSTABILITY AND ARC DEFLECTION

Chapter **Fel! Hittar inte referenskälla.** reports threshold values for residual magnetism that can give rise to arc instability and arc deflection. However, these values are given within fairly large ranges, and are not related to: the strength and type of the welding current (direct current or alternating current), the polarity (when direct current is used), the voltage of the welding current, type of electrode, type of material, etc. In order to examine the threshold values more closely for conditions that often apply when welding district heating pipes, the following experiments were carried out.

Two DN150 pipes, 700 mm long, were magnetized to a given level, and then welded together by a professional MMA welder. The welding was performed with Ø2.5 mm ESAB OK 48 DC+ electrodes. The welding machine was an EWM Picotig 200 pulse. The material thickness of the pipes was 4 mm and the steel grade P235GH. The straight edge was 1.5 mm, the gap width 2 mm and the joint angle 60°. The magnetization was carried out with two electric coils, placed in the middle of the pipes, see Figure 35 and Figure 36.

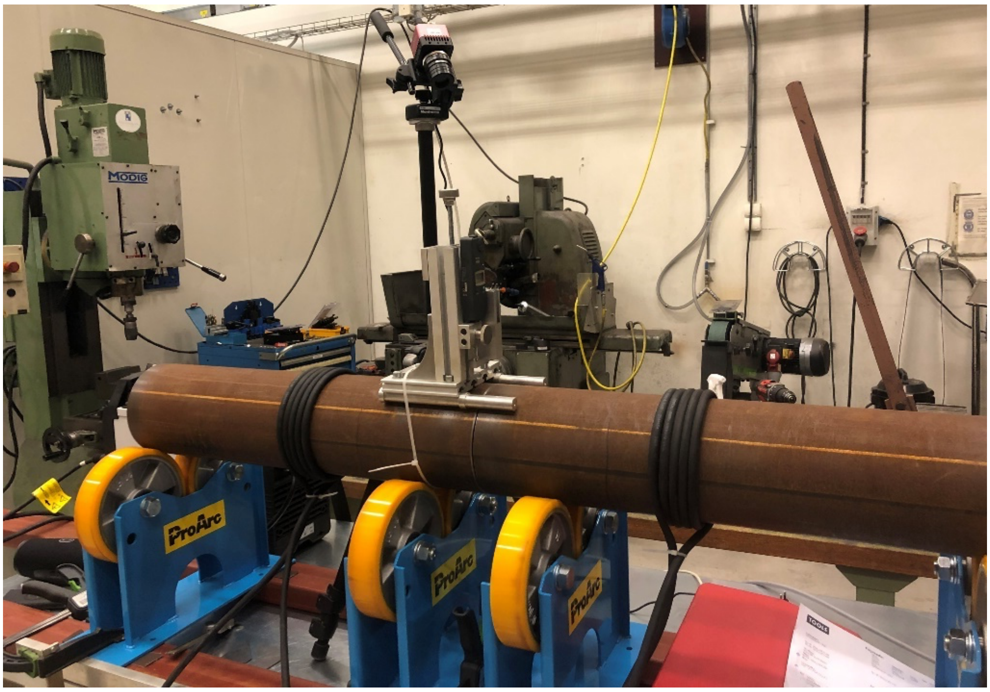

Figure 35. Experimental setup.

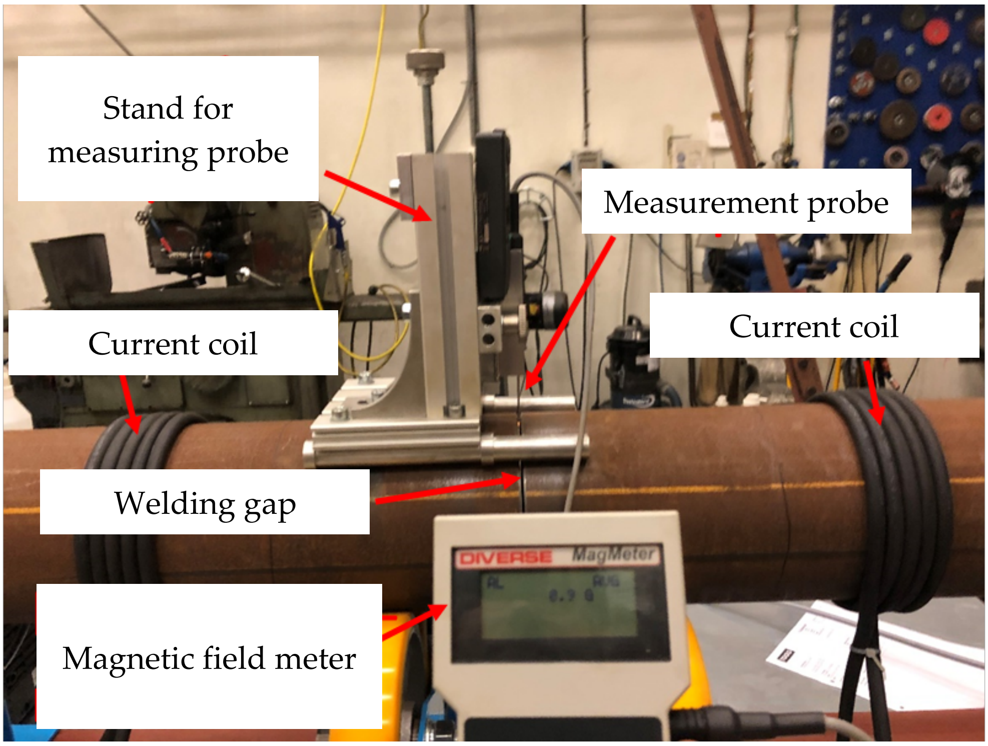

Figure 36. Experimental setup.

The coils are connected in series and wound in such a way that their magnetic fields which they create in the tubes are oriented in the same direction. The coils were fed with a direct current from the power source EWM Degauss 600 [17], see

Figure 37. The EWM Degauss 600 has a built-in demagnetization function where the demagnetization takes place by sending an alternating current with decreasing amplitude through the coils. That function was used to initially demagnetize the tubes prior to the prescribed magnetization. After the demagnetization, the maximum axial magnetic field in the welding gap could be reduced to a few Gauss. When the demagnetization was complete, a direct current was sent through the coils where the current strength was adjusted until the desired value of the magnetic field in the welding gap was reached. The desired magnetization was considered achieved when the maximum measured B_z-value coincided with the desired value. The magnetic field in the welding gap is measured with the measuring stand described in chapter **Fel! Hittar inte referenskälla.**.

The magnetic field in the weld gap created using the method described above exhibits small variations in the circumferential direction; the maximum variation of B_z in the circumferential direction is only a few Gauss when the magnetization level is between 5 – 100 G. Furthermore, the created magnetic field is not time dependent; once the magnetic field is adjusted to a given level, this level remains stable for more than 10 minutes (which was the control time) without the need to adjust the current in the coils.

Figure 37. EWM Degauss 600 [17].

When a specific magnetization level was achieved, the pipes were welded together using four tack welds. Then, a 100 mm section of the root pass was welded. The welder then assessed, on a ten-point scale, the difficulty of performing the various tack welds and the root pass based on the given magnetization level.

To further study the degree of arc instability and arc deflection at a certain magnetization level, the arc was filmed. For this purpose, the Photonfocus HD1-D1312-80-G2 camera with a frame rate of 54 frames per second was used. A NE05A in the series NE10A was used as a filter.

Additionally, the welding current and voltage were logged to analyze and provide insights of occurrence of arc instability and arc deflection.

5 Experimental result

In this chapter, results from experimental studies conducted in this project are presented. These results include findings from various magnetic field measurements as well as observations from tests related to arc instability and arc deflection.

5.1 MAGNETIC FIELD MEASUREMENTS

Magnetic field measurements were conducted on various district heating pipes at E.ON in Stockholm. The measurements were performed on three different pipes: one DN600 and one DN400 pipe from the manufacturer LOGSTOR, and one DN300 pipe from the manufacturer isoplus. During the measurements, the pipes were positioned in a pipe stand, as shown in Figure 38.

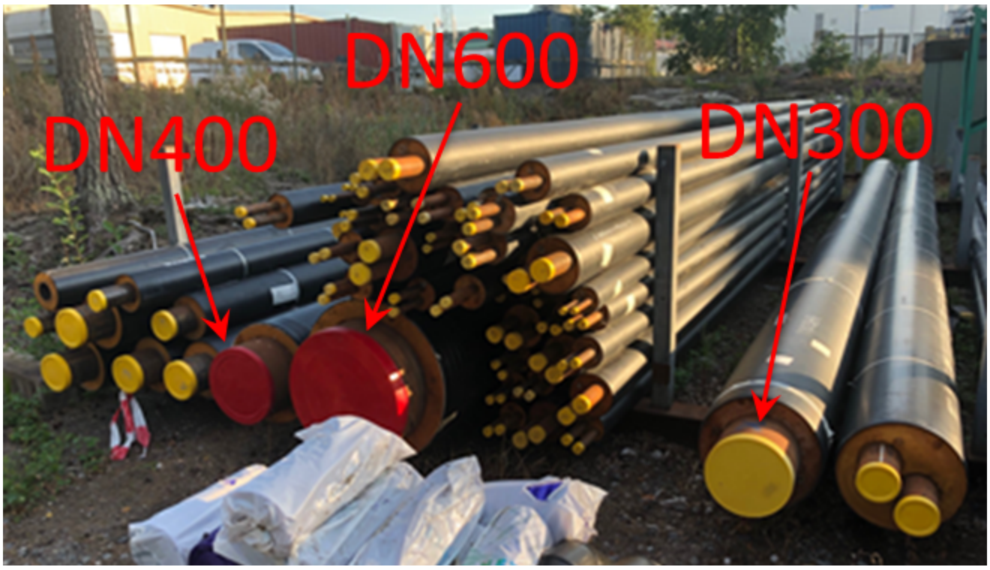

Figure 38. The three different pipes which the magnetic field measurements were performed on.

5.1.1 DN600 pipe

Data for the DN600 pipe is shown in Table 9 below.

Table 9. Data for DN600 pipe.

Pipetype	DN600, spiral welded
Manufacturer	LOGSTOR
Material	P235GH
Outer diameter	610 mm
Thickness	7.1 mm
Length	16 m
Straight edge	2 mm
Joint bevel angle	60°

Figure 39 shows the measured B_z-component for eight positions (angles) at each end of the pipe. The B_z -values given are the maximum values measured for the given angles. It has been determined by sweeping the probe over the straight edge in a radial direction for a given angle until the maximum value is found, which can be done in increments of a hundredth of a mm with the measuring stand in chapter **Fel! Hittar inte referenskälla.**. The polar coordinate systems in Figure 39 have a positive orientation (counter-clockwise) about an axis that points from 'pipe end 2' to 'pipe end 1'. Furthermore, B_z is positive in Figure 39 if the axial field points from 'pipe end 1' to 'pipe end 2'.

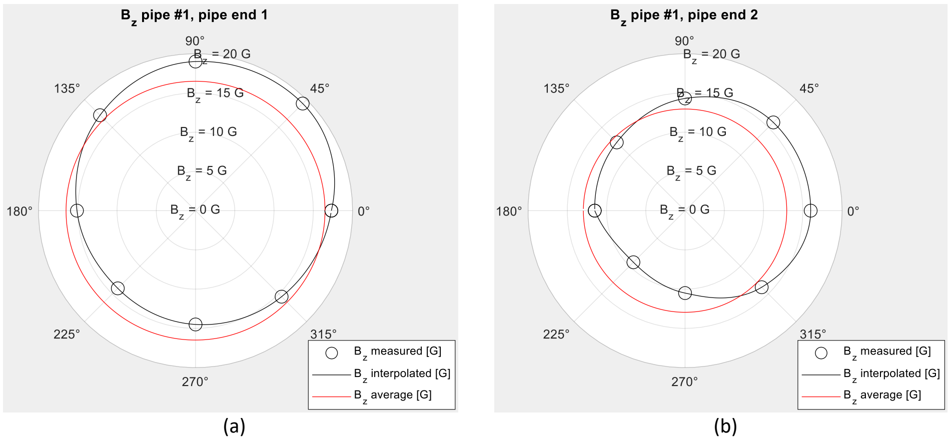

Figure 39. Measured maximum values of the $\boldsymbol{B_z}$-field for the DN600 pipe in eight positions for: (a) Pipe end 1, and (b) Pipe end 2.

From Figure 39 it can be seen that the B_z field varies slightly in a ring around both ends of the pipe. The maximum value is showing at approximately 45°, and the minimum value at approximately 225° for both pipe ends. The maximum and average values are 19 and 17 G respectively for end one, and 16 and 13 G respectively for end two. Note that the magnetic field at the pipe ends of the DN600 pipe can be affected by the closely surrounding pipes and that the pipe is close to the ground, see Figure 38.

5.1.2 DN400 pipe

Data for DN400 is shown in Table 10 below.

Table 10. Data för DN400 pipe.

Pipetype	DN400, straight welded
Manufacturer	LOGSTOR
Material	P235GH
Outer diameter	406 mm
Thickness	6.3 mm
Length	16 m
Straight edge	2 mm
Joint bevel angle	60°

The measured magnetic field for the DN400 pipe is shown in Figure 40. It is lower than for the DN600 pipe. The maximum and average values are 10 and 8 G respectively for 'pipe end 1', and 13 and 11 G respectively for 'pipe end 2'.

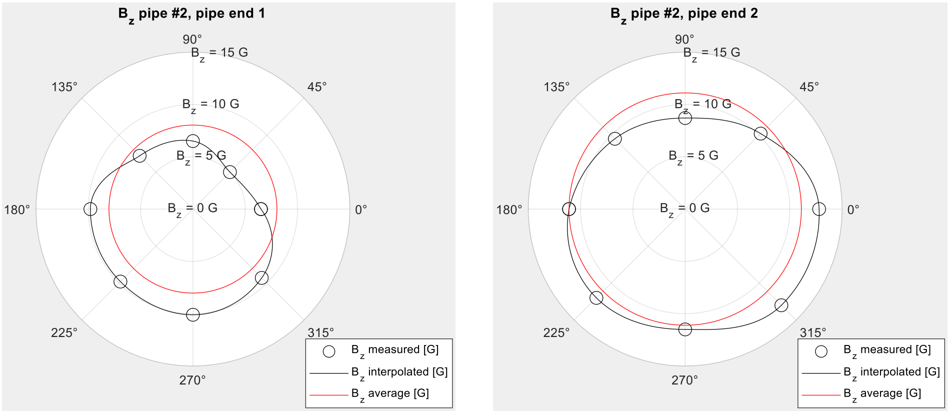

(a) (b)

Figure 40. Measured maximum values of the $\boldsymbol{B_z}$-field for the DN400 pipe in eight positions for: (a) Pipe end 1, and (b) Pipe end 2.

5.1.3 DN300 pipe

Data for the DN300 pipe is shown in Table 11 below.

Table 11. Data for DN300 pipe.

Pipetype	DN300, straight welded
Manufacturer	isoplus
Material	P235GH
Outer diameter	324 mm
Thickness	5.6 mm
Length	12 m
Straight edge	2 mm
Joint bevel angle	60°

The DN300 pipe is the one of the three pipes with the lowest magnetization. The maximum magnetization is below 5 G, see Figure 41.

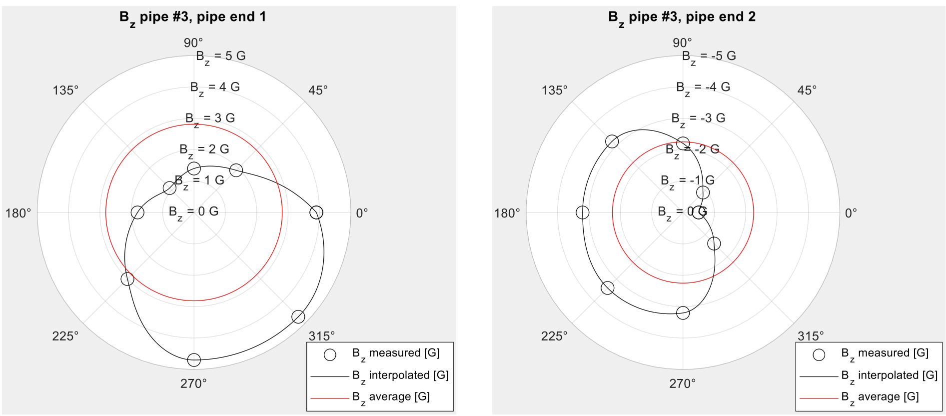

(a) (b)

Figure 41. Measured maximum values of the $\boldsymbol{B_z}$-field for the DN400 pipe in eight positions for: (a) Pipe end 1, and (b) Pipe end 2.

5.1.4 B_ϑ-component

The B_θ-component of the magnetic field was also measured for the three tubes above. However, it was always about three to five times less than B_z-component

5.2 THE INFLUENCE OF THE ISOLATION PROCESS ON THE MAGNETIZATION

It was not known whether magnetization can occur when the district heating pipes are insulated. To investigate this, measurements were made at the district heating pipe manufacturer Powerpipe Systems AB, which uses polyurethane foam insulation. Five DN250 pipes were examined, see Table 12 for pipe specification.

Table 12. Data for DN250 pipe.

Pipetype	DN250, straight welded
Manufacturer	Powerpipe
Material	P235GH
Outer diameter	273 mm
Thickness	5 mm
Length	16 m
Straight edge	2 mm
Joint bevel angle	60°

Before the pipes are insulated, the magnetic field is measured at both ends in the same way as previously described in chapter **Fel! Hittar inte referenskälla.** (but only in one place and not eight as before). Pipe length and measurement location were marked with a mark-pen on each pipe. After the isolation, the magnetic field is measured again in the same place as before the isolation. For all five tubes, the difference in the magnetic field before and after isolation was less than ±3 G for both ends, which is within the measurement error. The conclusion is therefore that no magnetization can be established from this insulation process of DN250 pipes.

5.3 THRESHOLD VALUES FOR ARC DEFLECTION

In this section, the results of the investigation into arc instability and arc deflection in DN150 pipes welded with DC+ using ESAB OK 48 electrodes are presented. The experimental setup is described in Chapter **Fel! Hittar inte referenskälla.**. Four different levels of magnetization were considered: 0, 20, 30, and 40 G.

5.3.1 Assessment Based on the Welder's Observations

Table 13 below indicates, on a ten-point scale evaluation, the welder's assessment of the difficulty of performing each tack weld and the 100 mm long root pass. A total of five experiments were conducted with different levels of magnetization. When the magnetization was below 40 G, the welding current was 84 A, and the voltage was 21 V. However, when the magnetization reached 40 G, the welder increased the welding current to 90 A (while keeping the voltage at 21 V) to gain better control over the arc. It's worth noting that the ESAB OK 48 welding electrode with a diameter of 2.5 mm has a recommended current range of 70 – 100 A.

Table 13. The difficulty assessment from welders.

	Degree of difficulty (1-10)				
	Residual magnetism (Gauss)				
	0	20	20	30	40
Tackweld 1	1	4-5	4-5	5-6	6-7
Tack weld 2	1	4-5	4-5	7-8	6-7
Tack weld 3	1	4-5	4-5	7-8	6-7
Tack weld 4	1	4-5	4-5	7-8	6-7
100mm weld	1	2-3	2-3*	4-5	5-6
* Difficult in start for 2-3					

When the magnetization was 0 G (demagnetized pipes), the welder could easily both tack and weld 100 mm of the root string, see the first column in Table 13. When the magnetization was 20 G, the welder could experience some problems with arc instability, especially during tack welding and at the start of the 100 mm long root pass, see columns two and three in Table 13. At 30 G magnetization, the welder felt that the tack weld was difficult to perform, see column four in Table 13. At 40 G, the tack weld was so difficult that the welder increased the welding current from 84 to 90 A. This facilitated the tack welding, which now became easier to perform than when the magnetization was 30 G, see column five in Table 13. However, it was a little more difficult to weld the 100 mm long root pass compared to 30 G magnetization.

5.3.2 Assessment based on filmed arc

The arc was filmed when the 100 mm long root pass was welded in order to study arc instability and arc deflection. From these films, a higher instability of the arc could be seen, with more weld spatter and uneven droplet transition, when the magnetization was 30 G or higher. At 40 G magnetization, arc deflection could sometimes be seen. The filmed arc for the 20 G magnetization could be seen to be slightly more disturbed than for the arc when the magnetization is zero. To study this in more detail, a camera with a higher frame rate and better background lighting must be used, which will be done in a follow-up project.

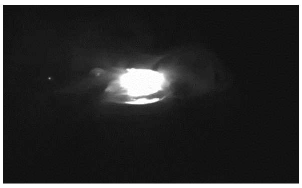
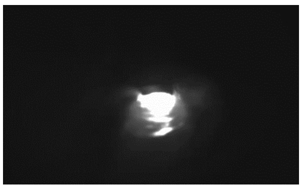
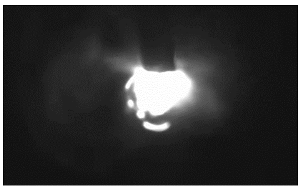

(a) (b) (c)

Figure 42. Images from filmed arc at: (a) 0 G, (b) 20 G, and (c) 40 G.

5.3.3 Assessment based on current and voltage log

The welding current and voltage were logged during the welding of the 100 mm root strand. Figure 43 shows the results of this when the sampling frequency is 4 kHz. Figure 44 shows a zoom in of the welding current and voltage from Figure 43c.

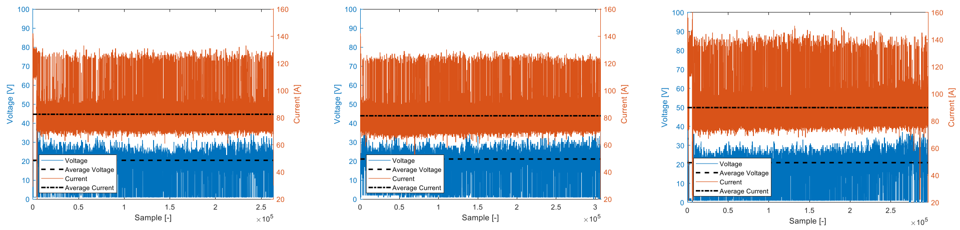

(a) (b) (c)

Figure 43. Welding current and voltage for the residual magnetization: (a) 0 G, (b) 20 G, and (c) 40 G.

Arc instability affects the drop transition and therefore also affects the welding current. Arc deflection affects the arc length, which in turn affects the welding voltage. A spectral analysis of the welding current and voltage may therefore provide valuable information about the degree of arc instability and arc deflection. Unfortunately, we never had time to study this in this project. It will be done in a continuation project.

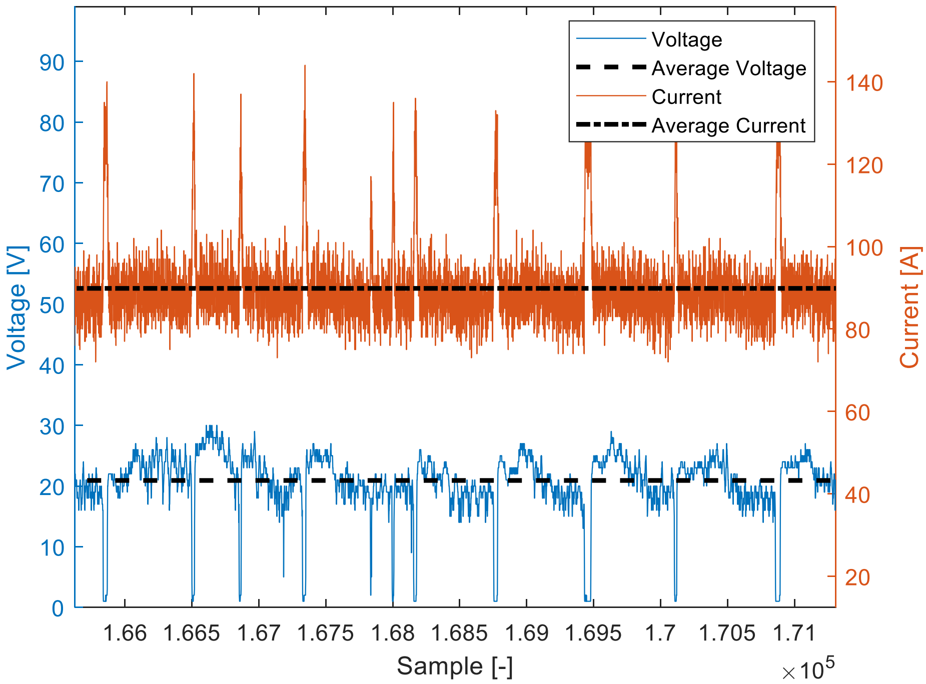

Figure 44. Welding current and voltage with residual magnetization of 40 G.

5.4 MAGNETIZATION DUE TO WELDING

It has been discussed whether magnetization can occur when the pipes are welded together. To investigate this, two 700 mm long DN150 pipes were welded together using a root pass. After the weld had cooled to room temperature, the magnetic field was measured at four points on each end of the two welded pipes. Subsequently, a second weld was made on the root pass. After the weld had cooled, magnetic field measurements were taken again at the same locations as before. Table 14 shows the results of the magnetic field measurements before and after the second weld. As seen from the table, the magnetic field changes by only 1 – 2 G due to the welding. This change is less than the measurement accuracy, and therefore, it can be concluded that welding in this case does not seem to create significant magnetization.

Table 14. Magnetization before and after welding of weld number two.

	Magnetism (Gauss)			
	Before weld two		After weld two	
Measurement position (°)	**Left end on pipe**	**Right end on pipe**	**Left end on pipe**	**Right end on pipe**
0	2	5	2	6
90	3	1	4	3
180	3	2	3	3
270	1	2	2	4

5.5 SUMMARY OF RESULT

The most important experimental results from this chapter are summarized here.

- Magnetic field measurements made on a DN600 district heating pipe showed a maximum field strength of approx. 20 Gauss at one end of the pipe. For a DN400 pipe, the maximum field strength is measured to about 15 Gauss at one pipe end, and for a DN300 pipe to about 5 Gauss at one of the pipe ends. For all three pipes, it was the case that the field strength varied in the ring. The annular component of the magnetic field was three to five times smaller than the axial component for all three tubes.
- Magnetic field measurements, made before and after pipe insulation of DN250 pipes at Powerpipe, have not been able to demonstrate that the insulation process can give rise to strong residual magnetism.
- Magnetic field measurements, carried out on DN150 pipes, have indicated that the welding process does not give rise to strong residual magnetism.
- Experimental trials have indicated that arc instability and arc deflection occur at approximately 20 and 40 Gauss respectively for DN150 pipes.

6 Magnetization at steel pipe manufacturers

The numerical results from Chapter 3 suggest that residual magnetism formed in district heating pipes from the magnetic field of the earth or electrical power lines is not strong enough to lead to problems with arc instability and arc deflection. It also seems doubtful that train and truck wagons, in which the pipes are transported, could be so strongly magnetized that they in turn magnetize the pipes to a level that could lead to welding problems. Note that numerical simulations in Chapter 3 have indicated that an axial field of 2 G, with an extent of tens of meters, is required to magnetize a tube to a level such that arc deflection can occur. It is unclear whether such oriented and extended magnetizations can exist in train and truck wagons. Furthermore, results from chapter **Fel! Hittar inte referenskälla.** indicate that it is also doubtful that magnetization can occur when several pipes are welded together. Results from Chapter 5.2 also indicate that the insulation process of district heating pipes does not result in significant magnetization. Assuming no magnetic lifting tools have been used after manufacturing, which is the case for pipes from manufacturers like Powerpipe, the above suggests that strongly magnetized district heating pipes is due to their magnetization during the steel pipe manufacturing process. This is further explored in the following section.

6.1 MAGNETIZED NON-DESTRUCTIVE TESTING

As previously described in Chapter **Fel! Hittar inte referenskälla.**, residual magnetization can occur in various ways during the manufacturing of steel pipes. In this chapter, we will take a closer look at magnetization from non-destructive testing, which can lead to very strong residual magnetization.

Steel pipe welds (spiral or longitudinal) and pipe ends are inspected using non-destructive testing methods. Various methods can be employed for non-destructive testing, including ultrasonics, X-rays, eddy current testing, or magnetic particle inspection. Different steel pipe manufacturers may use different combinations of these methods. Some manufacturers, for instance, use ultrasonics and X-rays to inspect pipe welds and pipe ends, respectively. Other manufacturers use eddy current testing and magnetic particle inspection to exam welds and ends. Eddy current testing and magnetic particle inspection are particularly interesting because they often require strong pre-magnetization of the pipe to perform these methods, meaning the pipe must be magnetized before these techniques can be used. Magnetization levels can exceed 100 G, and it’s important to demagnetize the pipe after the inspection is completed. Demagnetization can be achieved, for example, by passing the pipe through a demagnetization tunnel.

6.2 INVESTIGATION OF MAGNETIZATION AT STEEL PIPE MANUFACTURERS

In Europe, there are several steel pipe manufacturers that supply pipes for various purposes, including district heating pipes. To investigate whether these pipe manufacturers use magnetized non-destructive testing and how they handle demagnetization, the questionnaire below was sent out. The questionnaire was sent to pipe manufacturers that supply steel pipes to the district heating pipe manufacturer Poliurs.

Questions about the inspection methods for the pipe weld

1. Which method/methods are used to inspect the welds of the pipes?
2. Is every pipe's weld inspected?
3. If ultrasonic testing is performed, is a piezoelectric crystal transducer or an electromagnetic acoustic transducer used?
4. If eddy-current testing (ECT) is used:
    a. is full saturation ECT used?
    b. is it performed on every pipe, or just on some pipes per batch?
    c. if saturated ECT is used, how is the magnetization performed: locally around the weld or all over the pipe?
5. If particle magnetic inspection is used:
    a. is it performed on every pipe, or just on some pipes per batch?
    b. how is the magnetization performed: locally around the weld or all over the pipe?
    c. is the pipe magnetized in both longitudinal and circumferential directions?

Questions about demagnetization

1. Is every pipe demagnetized?
2. If demagnetization is performed:
    a. how is the demagnetization performed: manually or automatically?
    b. is the demagnetization performed locally around the weld, or all over the pipe? Is this different between spiral and straight welded pipes?
    c. what is the name of the demagnetization equipment that is used in the plant?
    d. is the residual magnetism measured after demagnetization? If so:
        i. how often is it measured: on every pipe, or for some pipes per batch?
        ii. are the different components of the magnetic field measured (i.e. longitudinal, circumferential, and radial components)?
        iii. where on the pipe are the measurements done, and what are the maximum levels that are accepted?
        iv. is beveling performed before or after demagnetization?
        v. is the residual magnetism measured on the root face? If so, what are the maximum allowed value there?
        vi. if the allowed residual magnetism on the root face is allowed to be larger than 5 – 7 Gauss, would it be possible with the existing demagnetization equipment to decrease it to 5 – 7 Gauss?
        vii. are magnetic lifting tools used after demagnetization has been performed? If so, has it been checked how much the magnetic lifting tool magnetize the pipe?
3. Are magnetic lifting tools used during or after the manufacturing process?
4. Are there any steps in the pipe manufacturing process that are known to cause residual magnetization?

Three of the steel mills responded to the questionnaire, and their responses are attached in Appendix A to this report. We have chosen to keep their names anonymous and refer to them as Steel Mill 1, Steel Mill 2, and Steel Mill 3. A brief summary of their responses is provided in Table 15 below.

Table 15. Summary of the steel mills' response to the questionnaire.

Question	Manufacture 1	Manufacture 2	Manufacture 3
Is eddy current testing used?	Yes	No	No
Is Magnetic particle inspection (MPI) used?	Yes	Yes	No
Do you demagnetize every pipe?	Yes	No, only for MPI tested pipe	No
What is the maximum level of the demagnetization?	~20 Gauss	~30 Gauss	-
Is it possible to demagnetize the pipe to 5-7 Gauss?	Yes	No	-

Steel Mill 1 indicated that they use both eddy current testing and magnetic particle inspection, and they demagnetize each pipe. Steel Mill 2 stated that they use magnetic particle inspection and demagnetize each pipe tested. Steel Mill 3 does not use magnetized non-destructive testing and does not have a demagnetization process.

From Table 15 and the responses in the appendix, it is evident that demagnetization after non-destructive testing can reduced the residual magnetism to the levels about 20 – 30 G. A similar level was found for another steel mill after reviewing inspector certificates from about ten steel mills made accessible through E.ON. Among these steel mills, only one specified an upper limit for residual magnetization in its inspection certificate, which was set at 30 G. It should be noted that, in the worst case, if one pipe end has magnetization of 20 G (north pole) and is joined with another pipe end magnetized to -20 G (south pole), the magnetic field in the weld seam will significantly exceed 40 G, as understood from Section 3.2. Furthermore, the experiments in Section 5.3 show that problems with arc deflection begin to occur at around 40 G. The maximum limits of 20 – 30 G for residual magnetism that the steel mills allow are therefore too high if one wants to be completely sure of avoiding arc deflection issues.

7 Recommendations

In this chapter, suggestions are given on how problems with arc instability and arc deflection in district heating pipes can be reduced.

7.1 CHANGE OF TECHNICAL PROVISIONS

In the previous chapter it was shown that steel pipe manufacturers can allow residual magnetizations of up to 30 G, which can lead to problems with arc deflection. Currently, there is no standard where a maximum permissible limit for residual magnetization in district heating pipes is specified. However, it is stated in the energy companies' technical regulation D:211 Läggningsanvisningar (Laying instructions) [18]: "*Vidare bör den tilltänkta tillverkaren/leverantören kunna garantera att magnetfältet från eventuell restmagnetism I stålrören inte överstiger 20 Gauss*" ("Furthermore, the intended manufacturer/supplier should be able to guarantee that the magnetic field from any residual magnetism in the steel pipes does not exceed 20 Gauss"). We consider this to be too high a magnetization. If, in the worst case, a pipe end that is a magnetic north pole with a magnetization of 20 G is brought together with a pipe end that is a magnetic south pole with a magnetization of -20 G, the magnetic field in the weld gap will be well above 40 G, which can cause problems with arc deflection (note that district heating pipes cannot be rotated in any way in relation to each other as they have moisture alarms that need to be matched, therefore you may be forced to mount pipe ends with different magnetic polarities). Experimental trials in this work have shown that arc deflection starts to become a problem around 40 G in the weld gap (see section 5.3). Furthermore, the numerical calculations in Chapter 3 show that the magnetic field at the right edge is amplified more than eight times when the tubes are brought together. Thus, to avoid arc deflection, the residual magnetism must not be higher than about 5 G at the straight edge (before the tube is brought together with the other tube).

To address this issue, recommendations for maximum limits on residual magnetism allowed after demagnetization will be developed. This will be carried out in a follow-up project funded by Energiforsk. The maximum limits will depend on factors such as pipe type (diameter, wall thickness, etc.), type of welding electrode, welding method (AC or DC), and more. These limits will be determined using the experimental setup developed in Section **Fel! Hittar inte referenskälla.** of this report. It emphasizes the importance of further developing the experimental setup to eliminate the subjective human assessment factor. This can be achieved by objectively determining the degree of arc instability/arc deflection through methods such as high-speed filming of the arc or spectral analysis of the welding current and voltage, rather than relying on the welder's assessment, as done in Section **Fel! Hittar inte referenskälla.**. It is hoped that when steel mills demagnetize their pipes to these established maximum limits, problems with arc deflection will be reduced.

7.2 MAGNETIC FIELD MEASUREMENT AT DISTRICT HEATING PIPE MANUFACTURERS

If a steel mill cannot demagnetize to the recommended level, an alternative may be for the district heating pipe manufacturer to measure the magnetism and mark it on the pipe. This can be done very quickly with the measuring stand developed in this report; measuring the magnetism in four positions on a pipe end can be done in about 10 s. Based on the marking on the pipe of the degree of magnetization, the welder can then assess how difficult it will be to perform the welding even before he starts the actual welding. If the magnetization is high, he can then, for example, choose to use one of the methods in section **Fel! Hittar inte referenskälla.** or **Fel! Hittar inte referenskälla.** below.

7.3 WELDING THE ROOT PASS WITH ALTERNATING CURRENT

As the residual magnetism is high, the root pass can be welded with alternating current instead of direct current. This is because alternating current welding is less sensitive to arc deflection than direct current welding. However, alternating current welding is a secondary option under normal conditions because direct current welding then has a more controllable arc, less welding spatter, easier starting and is easier to weld vertically with.

7.4 USE OF DEMAGNETIZATION EQUIPMENT

At very high levels of residual magnetism, demagnetization equipment, for example of the type in the test set-up in section **Fel! Hittar inte referenskälla.**, must be used. The disadvantage is that such equipment can be expensive, difficult to transport, especially if the welding takes place down in a pipe trench, and that it can take time to set up equipment: e.g. wrap the coils around the pipes.

8 Conclusions

In this work, a numerical calculation model has been developed to study the magnetic field in and around steel pipes. A measuring stand has been developed to quickly and robustly measure the magnetic field at pipe ends and in the weld gap between two district heating pipes. An experimental setup has been developed to investigate threshold values of residual magnetism required to cause arc instability and arc deflection. Some of the key findings from this work can be summarized as follows.

Numerical calculation:

- Numerical calculations show that the magnetic field in the weld gap is much stronger than it is at the pipe ends before the pipes are brought together. This is important to take it into account when measuring the risk of arc deflection on pipes forehand.
- Numerical calculations show that the magnitude of the magnetic field in the weld gap and at the right edge is well represented by the amount of the axial component (B_z) when the pipes have been magnetized by an axial background field. Thus, if the component of the magnetic field in the annular direction is small compared to that in the axial direction (which is true for all experimental measurements in this work), the magnetic field can be quantified both in the weld gap and at the straight edge by measuring only the axial component.
- Numerical calculations indicate that the magnetic fields of the earth and power lines have a small influence on the residual magnetism in district heating pipes.
- Numerical simulations show that the magnetic field in the weld gap is moderately dependent on the pipe diameter, the size of the straight edge (nose) and the joint bevel angle. However, it is strongly dependent on the material thickness and the gap width. It is also strongly dependent on the pipe length when the length is less than 10 m, after which the dependence decreases almost completely.

Magnetic field measurements:

- Magnetic field measurements on DN250 pipes have shown that the insulation process (used in Powerpipe, i.e. polyurethane foam insulation) does not give rise to any residual magnetism.
- Magnetic field measurements on DN150 pipes have shown that when a second weld is placed on the root pass, it does not produce magnetization. Thus, the welding process itself does not seem to give rise to magnetization.

Experimental investigations:

- Experimental trials have indicated that arc instability and arc deflection occur at approximately 20 and 40 G respectively for DN150 pipes, when they are welded with an OK 48 electrode with a diameter of 2.5 mm.

- A survey shows that there are steel mills that demagnetize their pipes down to 20 – 30 G after performing magnetized non-destructive testing. These are insufficient demagnetization levels for arc deflection to be completely avoided.

Recommendations:

- Maximum permissible limits for the residual magnetism after demagnetization will be developed in a continuation project granted by Energiforsk. This will be done with methods developed in this project, and with respect to pipe dimension and welding method. The hope is that this can provide a basis for the steel mills at the levels they should demagnetize to, so that the problems with arc deflection can be avoided.

9 Future work

The work in this report has primarily been focused on the development of a simple numerical calculation model that can be used to increase knowledge of the magnetic field in the weld gap between magnetized steel pipes. This is to develop measurable methods for controlling the risk of arc deflection, but also to develop experimental setups to find threshold values for the field strength when arc deflection occurs. A project continuation has been granted through the project "Futureheat–- Svetsbarhet av fjärrvärmeapplikationer, en fortsättningsstudie". In the continuation project, the focus will shift towards mapping residual magnetism in district heating pipes as well as producing threshold values for arc deflection for several different pipe types and welding methods. The following subjects are planned to be studied.

- *Mapping*: An extensive survey is planned to be carried out, where district heating pipes that have had problems with arc deflection are mapped. It will be investigated whether there is any connection between district heating pipes with high residual magnetization and the followings:
    - *Steel Pipe Manufacturers*: Which steel mills produce pipes with high residual magnetism? What does the production process look like at these steel mills?
        - Is magnetized non-destructive testing used?
        - Are the pipes demagnetized, and if so, to what level?
        - Is magnetic lifting equipment used, and if so, has it been ensured that residual magnetism cannot occur as a result of this?
    - *Transportation*: How have pipes with high residual magnetism been transported?
        - Have the pipes been transported by train, truck, or both?
        - Have magnetic lifting tools been used during loading or unloading, and if so, has it been ensured that residual magnetization cannot occur as a result of these tools?
        - Have the pipes been stored at an intermediate storage location?
    - *Insulation Manufacture:* Which insulation manufacturers supply pipes with high residual magnetism? What does the production process look like at these insulation manufacturers?
        - Is the insulation process used capable of causing residual magnetism?
        - If magnetic lifting equipment is used, has it been verified that residual magnetization cannot occur?

- *Threshold values for arc deflection*: Robust methods based on arc filming and spectral analysis of welding current will be developed to determine threshold values when arc instability and arc deflection occur. This will be done with respect to:
    - *Pipe type (diameter, wall thickness, etc.), material type.*
    - *Type of welding electrode.*
    - *Welding method: direct current or alternating current.*
- *Magnetic field measurement and numerical calculation:*
    - Numerical calculations in this work show that the magnetic field gradient, for example, at the corners of the straight edge, can be very high. Since the sensor in the probe of a magnetic field meter has a certain spatial extent, it will measure the average of the magnetic field over certain volume. Therefore, it is uncertain how well a particular magnetic field probe can resolve the magnetic field. This is very important to understand when measuring threshold values for arc instability. Threshold values should be independent of which magnetic field probe is used. This will be studied in the continuation project. It will also be studied what should be measured to determine the threshold value: should it be the maximum value in the weld gap, should it be a value from a fixed point, for example, 1 mm above the upper corner of the straight edge, or should it be an average value calculated over a certain volume?
    - In this work, the magnetization that causes one pipe end to be a magnetic north pole and the opposing pipe end to be a magnetic south pole has been considered the worst case because it is believed to cause the most deflection of the plasma. However, it is also very important to consider the case when both pipe ends in the weld gap have the same magnetic polarity (i.e., north-north or south-south).
    - It is also essential to consider the temperature dependence of magnetic permeability when investigating threshold values for arc deflection. Since magnetic permeability decreases with increasing temperature, this can lead to an amplification of the magnetic field in the cold region in front of the arc. This can result in very high magnetic fields, for example, just before the end of the root pass. This phenomenon must be taken into account when determining threshold values.
    - To assess the risk of arc deflection, you can measure the magnetic field at the pipe ends before they brought together, taking into account the amplification factor. Typically, the pipes are stacked, close to the ground, or in a pipe trench in such scenarios. When

measuring at the pipe ends in these conditions, it's essential to understand how these factors affect the measurement results.

- Numerical calculations from this work have indicated that the Earth's and power lines' magnetic fields have a minimal impact on the magnetization of district heating pipes. This needs validation. For instance, you can measure the magnetic field at pipe ends as a function of the pipe's angle relative to a meridian line, to study the effect of the Earth's magnetic field. Or you can measure the magnetic field before and after the pipe has been transported under a power line.
- The smallest hysteresis used in calibrating the numerical calculation model in this work had a value of $H_p = 385$ A/m, which was the lowest value that the hired laboratory could handle. This is a relatively high value, and it would be beneficial if the model could also be calibrated against hysteresis with $H_p = 100$ A/m and $H_p = 10$ A/m to improve the model's accuracy at low magnetizations.
- The calculation model in this work does not consider time-dependence. It was calibrated against hysteresis curves generated from a magnetic field varying at a frequency of 0.5 Hz. Time-dependence should be studied in future research by examining hysteresis produced at different frequencies.
- The time-dependence of the magnetic field in a district heating pipe has not been investigated in this work. In future work, it would be very interesting to explore how it varies over time, from days and weeks to months and years.

10 Acknowledgement

The authors are very grateful for the funding provided by Energiforsk and would like to extend special thanks to the following individuals:

- The project's reference group consisting of: Harald Andersson (E.ON), Anders Fransson (Göteborg energi), Martin Linder (Tekniska Verken) och ordförande Magnus Ohlsson (Öresundskraft), for all the interesting and informative discussions, and for all the pleasant meetings.
- Mattias Igestrand, research engineer at the University West, for sharing his deep knowledge in welding and for all the help in setting up the experimental equipment.
- Östen and Josefine Karlsson, Ställbergs Mekaniska AB, for letting us to borrow their workshop to manufacture the measuring fixture .
- Peter Norberg, Svetsmaskinservice AB, for lending demagnetizing and welding equipment and sharing his extensive knowledge about welding issues related to residual magnetism .
- Karin Liljegren, Powerpipe, for sharing her deep knowledge in district heating pipes and for the very pleasant visit to Powerpipe. And for all the pleasant and informative phone calls. A huge thank you as well for the pipes we received for the experiments, and for the material we received for the toroids.
- Niclas De Lorenzi, Stockpipe AB, for engaging discussions on residual magnetism in district heating pipes, for distributing our magnetism questionnaire to steel pipe manufacturers, and for providing us with welding data used in the experiments on arc deflection. A huge thank you as well for sharing your knowledge about the technical provision D:211.
- Stig Vikner, AB Alvenius Industries, for the very pleasant visit to Alvenius where we got to see how spiral-welded pipes are manufactured and for allowing us to perform magnetic field measurements in the production area.
- Elisabet Bredin Petterson, E.ON, for arranging the magnetic field measurements on district heating pipes and for providing us access to inspection certificates from several different steel pipe manufacturers.
- Jonas Ohlsson, Kjell Hurtig, Mats Högström, research engineers at the University of West, for all the insightful discussions, assistance in the workshop, and help with various tasks.
- Morgan Nilsen, Associate Professor at the University of West, for lending the camera for the experiments on arc deflection and for assistance in setting it up.

Energiforsk

11 Appendix A

This appendix contains responses from the steel mills that responded to the questionnaire in section **Fel! Hittar inte referenskälla.**.

11.1 RESPONSE FROM THE STEEL PLANT 1

Questions about the inspection methods for the pipe weld

1. Which method/methods are used to inspect the welds of the pipes? **UT/ET/VT**
2. Is every pipe's weld inspected? **Yes**
3. If ultrasonic testing is performed, is a piezoelectric crystal transducer or an electromagnetic acoustic transducer used? **Piezoelectric**
4. If eddy-current testing (ECT) is used:
    a. is full saturation ECT used? **YES**
    b. is it performed on every pipe, or just on some pipes per batch? **Every pipe**
    c. if saturated ECT is used, how is the magnetization performed: locally around the weld or all over the pipe? **All over the pipe**
5. If particle magnetic inspection is used:
    a. is it performed on every pipe, or just on some pipes per batch? **1 pipe per strip**
    b. how is the magnetization performed: locally around the weld or all over the pipe? **All over the pipe**
    c. is the pipe magnetized in both longitudinal and circumferential directions? **circumferential directions**

Questions about demagnetization

1. Is every pipe demagnetized? **Yes**
2. If demagnetization is performed:
    a. how is the demagnetization performed: manually or automatically? **automatically**
    b. is the demagnetization performed locally around the weld, or all over the pipe? Is this different between spiral and straight welded pipes? **all over the pipe, we don't have spiral welded pipes**
    c. what is the name of the demagnetization equipment that is used in the plant? **Pruftechnik**
    d. is the residual magnetism measured after demagnetization? If so: **Yes**
        i. how often is it measured: on every pipe, or for some pipes per batch? **1 pipe per strip**
        ii. are the different components of the magnetic field measured (i.e. longitudinal, circumferential, and radial components)? **not applicable**
        iii. where on the pipe are the measurements done, and what are the maximum levels that are accepted? **at the end of the pipe, maximum levels that are accepted is according to customer's order**
        iv. is beveling performed before or after demagnetization? **Before, but the measurements are after beveling**
        v. is the residual magnetism measured on the root face? If so, what are the maximum allowed value there? **Yes, according to customer's order**
        vi. if the allowed residual magnetism on the root face is allowed to be larger than 5 – 7 Gauss, would it be possible with the existing demagnetization equipment to decrease it to 5 – 7 Gauss? **Yes, but we don't confirm this to customers**
        vii. are magnetic lifting tools used after demagnetization has been performed? If so, has it been checked how much the magnetic lifting tool magnetize the pipe? **No,**
3. Are magnetic lifting tools used during or after the manufacturing process? **No**

11.2 RESPONSE FROM THE STEEL PLANT 2

Questions about pipe weld inspection methods

1. What method / methods are used to inspect pipe welds? -

Answer: ultrasonic testing method

2. Is the weld seam of each pipe checked?

Answer: weld inspection is performed on each pipe

3. If ultrasonic testing is performed, is a piezoelectric crystal transducer or an electromagnetic acoustic transducer used?

Answer: using a piezoelectric transducer

4. If eddy current testing (ETC) is used:

Answer: VTK is not used in the production of pipes at the 159-529 mill

and. is full saturation ECT used?

b. is this done on every pipe or only on a few pipes in a batch?

c. If saturated ECT is used, how is magnetization performed: locally around the weld or throughout the pipe?

5. If magnetic particle control is used:

Answer: magnetic particle inspection is used to control the base metal of the end sections (as agreed)

and. is this done on every pipe or only on a few pipes in a batch?

Answer: on each pipe

b. How is magnetization performed: locally around the weld or throughout the pipe?

Answer: local magnetization - at the end sections of the pipes

c. Is the pipe magnetized in both the longitudinal and circumferential direction?

Answer: longitudinal magnetization

Demagnetization questions

1. Is each pipe demagnetized?

Answer: each pipe is demagnetized when using magnetic particle inspection.

Equipment for demagnetizing pipes "PTS", produced in the Czech Republic, is installed at the site of magnetic particle inspection.

2. If demagnetization is in progress:

and. How is demagnetization performed: manually or automatically?

Answer: automatically

b. Is demagnetization performed locally around the weld or across the entire pipe? What is the difference between spiral and straight welded pipes?

11.3 RESPONSE FROM THE STEEL PLANT 3

Questions about the inspection methods for the pipe weld

1. Which method/methods are used to inspect the welds of the pipes?
   Round tubes: OD 60,3-114,3mm: ultrasonic testing on the weld seam (optional: full body eddy current testing) + high pressure hydrotesting
   Round tubes: OD 114,3-219,1mm: ultrasonic testing on the weld seam + high pressure hydrotesting
2. Is every pipe's weld inspected?
   Yes
3. If ultrasonic testing is performed, is a piezoelectric crystal transducer or an electromagnetic acoustic transducer used?

4. If eddy-current testing (ECT) is used:
   a. is full saturation ECT used?
      No, we are testing only ferritic/magnetic materials (black steel)
   b. is it performed on every pipe, or just on some pipes per batch?
      Every pipe
   c. if saturated ECT is used, how is the magnetization performed: locally around the weld or all over the pipe?
      ----
5. If particle magnetic inspection is used:
   a. is it performed on every pipe, or just on some pipes per batch?
   b. how is the magnetization performed: locally around the weld or all over the pipe?
   c. is the pipe magnetized in both longitudinal and circumferential directions?

Questions about demagnetization

1. Is every pipe demagnetized?
   No, it is not necessary.
2. If demagnetization is performed:
   a. how is the demagnetization performed: manually or automatically?
   b. is the demagnetization performed locally around the weld, or all over the pipe? Is this different between spiral and straight welded pipes?
   c. what is the name of the demagnetization equipment that is used in the plant?
   d. is the residual magnetism measured after demagnetization? If so:
      i. how often is it measured: on every pipe, or for some pipes per batch?
      ii. are the different components of the magnetic field measured (i.e. longitudinal, circumferential, and radial components)?
      iii. where on the pipe are the measurements done, and what are the maximum levels that are accepted?
      iv. is beveling performed before or after demagnetization?
      v. is the residual magnetism measured on the root face? If so, what are the maximum allowed value there?
      vi. if the allowed residual magnetism on the root face is allowed to be larger than 5 – 7 Gauss, would it be possible with the existing demagnetization equipment to decrease it to 5 – 7 Gauss?

12 References

[1] S. Kou, Welding Metallurgy, Wiley, 2002.

[2] F. F. Chen, Introduction to plasma physics and controlled fusion, Springer, 2006.

[3] Diverse Technologies, [Online]. Available: https://diverse-technologies.net/arcblow-background/.

[4] EWM, [Online]. Available: https://www.ewm-group.com/assets/docs/PracticalGuide_Degaussing_EN.pdf.

[5] J. Coey, Magnetism and Magnetic Materials, Cambridge University Press, 2019.

[6] Wikipedia, [Online]. Available: https://en.wikipedia.org/wiki/Magnetic_domain.

[7] National Pipe Company Ltd, [Online]. Available: http://www.npc.com.sa/company/info/longitudinal_pipe/.

[8] IBSQ, [Online]. Available: https://ibsqjsc.com/pipeline/.

[9] Comsol AC/DC Module User's Guide, Version: Comsol 5.5, Comsol AB, 2019.

[10] J.-M. Jin, The Finite Element Method in Electromagnetics ^{3r}d Edition, Wiley-IEEE Press, 2014.

[11] D. J. Griffiths, ntroduction to Electrodynamics ^{4t}h Edition, Cambridge University Press, 2017.

[12] D. Jiles, Introduction to Magnetism and Magnetic Materials ^{3r}d Edition, CRC Press, 2015.

[13] LINKUN, [Online]. Available: http://se.lksteelpipe.com/news/what-s-p235gh-material-23439296.html.

[14] British Geological Survey, [Online]. Available: http://www.geomag.bgs.ac.uk/education/earthmag.html.

[15] Stuk, [Online]. Available: https://www.stuk.fi/web/sv/teman/eloverforing-och-kraftledningar/kraftledningar-orsakar-elektriska-och-magnetiska-falt.

[16] Diverse Technologies, [Online]. Available: https://diverse-technologies.net/magmeter-mf300h/.

[17] EWM, [Online]. Available: https://www.ewm-sales.com/sv/Degaussing/Set_Degauss_600--091-002065-00502.html.

[18] Energiföretagen, [Online]. Available: https://www.energiforetagen.se/forlag/fjarrvarme/d211-laggningsanvisningar/.

Keywords

Arc deflection, Residual magnetism, Magnetic field measurement, Pipe welding, Weldability, District heating pipes, Magnetostatics, Comsol, Jiles-Atherton, ALE.

WELDABILITY OF DISTRICT HEATING APPLICATIONS

Residual magnetism can cause major problems when welding district heating applications. If the residual magnetism is high enough, it can affect the arc, and thus cause welding defects. Since welding is one of the most important methods of joining district heating applications, it is therefore important to have control over residual magnetism levels so that welding defects can be avoided.

In this project, a numerical calculation model has been developed to investigate magnetic fields in district heating pipes. The model has been used to investigate the strength of the magnetized field required to magnetize a district heating pipe to such a level that problems can arise during welding. The model has also been used to study the influence of the magnetic field of the earth and power lines on the residual magnetism in district heating pipes. In this project, a robust measurement method has also been developed to measure the magnetic field at pipe ends and in the weld gap between two district heating pipes. An experimental method to investigate threshold values of magnetic field strength required to cause welding problems has also been developed.